"Method for the Measurement of Atmospheric Boil" (with James L. Harris), J. Opt. Soc. Am. **47**, 1056(A) (1957).
"Image Transmission by the Troposphere. I" (with A. R. Boileau and R. W. Preisendorfer), J. Opt. Soc. Am. **47**, 499 (1957).
"Atmospheric Limitations on Missile Photography," J. Soc. Motion Picture Television Engrs. **67**, 231 (1958).
"The Reduction of Contrast by Atmospheric Boil" (with W. H. Culver, W. H. Richey, and R. W. Preisendorfer), S.I.O. Reference 58-35 (1958).
"Nomographs for Calculating Visibility by Swimmers. I. Natural Light," Rept. No. 3-1, Contract NObs-72039 (1958).
"Aerial Measurements of Atmospheric Clarity and Sky Luminance near Alamogordo, New Mexico," Rept. No. 2-1, Contract NObs-72039 (1958).
"Photometry of the Sky at High Altitudes" (with A. R. Boileau and D. G. Simons), J. Opt. Soc. Am. **48**, 873 (1958).
"Luminance of the Horizon Sky at High Altitudes" (with D. G. Simons), J. Opt. Soc. Am. **48**, 282(A) (1958).
"Notes on Course Deception Principles," Rept. No. 3-8, Contract NObs-72039 (1959).
"Field Test of Underwater Visibility Predictions" (with J. E. Tyler and J. H. Taylor), J. Opt. Soc. Am. **49**, 1134(A) (1959).
"Nomographs for Calculating Visibility by Swimmers," J. Opt. Soc. Am. **49**, 510(A) (1959).
"Photometry during Manhigh III Balloon Flight" (with A. R. Boileau), S.I.O. Reference 59-25 (1959).
"Field Test of a System for Predicting Visibility by Swimmers from Measurements of the Clarity of Natural Waters" (with J. E. Tyler and J. H. Taylor), S.I.O. Reference 59-39 (1959).
"Examples of Water Clarity Data," Rept. No. 3-7, Contract NObs-72039 (1959).
"The Underwater Radiance Distribution Problem," Rept. No. 3-6, Contract NObs-72039 (1959).
"Examples of Water Clarity Data. II," Rept. No. 5-7, Contract NObs-72039 (1960).
"New Nomographs for Calculating Visibility by Swimmers," J. Opt. Soc. Am. **50**, 504(A) (1960).
"Irradiance from a Submerged Spherical Source," J. Opt. Soc. Am. **50**, 1130(A) (1960).
"A Compressed-Scale System of Portable Visibility Lights" (with J. J. Rennilson, R. W. Austin, and J. H. Taylor), S.I.O. Reference 60-16 (1960).
"Maps of Sky Luminance at Various Altitudes" (with A. R. Boileau, J. I. Gordon, and J. L. Harris), S.I.O. Reference 60-12 (1960).
"Status of Research on Underwater Photography by Artificial Light," S.I.O. Reference 60-23 (1960).
"Measurements of the Transmission of Light from an Underwater Source having Variable Beam Spread," S.I.O. Reference 60-57 (1960).
"Measurements of the Transmission of Light from an Underwater Point Source," Rept. No. 5-11, Contract NObs-72039 (1960).
"Derivation of the Contract Reduction Equation," Rept. No. 5-6 Contract NObs-72039 (1960).
"Flight Tests of an Airborne Light-Scattering Refractometer" (Interim Report), Rept. No. 4-1, Contract NObs-72039 (1960).
"Evaluation of an Airborne Light-Scattering Refractometer" (Final Report), Rept. No. 4-2, Contract NObs-72039 (1961).
"Irradiance from an Underwater Source having Variable Beam Spread," J. Opt. Soc. Am. **51**, 483 (1961).

Light in the Sea*

SEIBERT Q. DUNTLEY
Visibility Laboratory, Scripps Institution of Oceanography, La Jolla, California
(Received 27 August 1962)

Light in the sea may be produced by the sun or stars, by chemical or biological processes, or by man-made sources. Serving as the primary source of energy for the oceans and supporting their ecology, light also enables the native inhabitants of the water world, as well as humans and their devices, to see. In this paper, new data drawn from investigations spanning nearly two decades are used to illustrate an integrated account of the optical nature of ocean water, the distribution of flux diverging from localized underwater light sources, the propagation of highly collimated beams of light, the penetration of daylight into the sea, and the utilization of solar energy for many purposes including heating, photosynthesis, vision, and photography.

INTRODUCTION

An interest in the aerial photography of shallow ocean bottoms prompted the author to begin, nearly 20 years ago, a continuing experimental and theoretical study of light in the sea. Some of the principles discovered or extended and generalized by the author and his colleagues are summarized in this paper. Early discussions with E. O. Hulbert and D. B. Judd as well as publications by many investigators[1] provided a valuable starting point. By 1944 the author was using a grating spectrograph, specially designed by David L. MacAdam, in a glass-bottomed boat off the east coast of Florida to obtain the spectroradiometric data shown in Fig. 1; the presence of reefs and sandy shoals show clearly in the green region of the spectrum.[2] When the spectrograph was flown in an airplane 4300 ft above the same ocean locations, the radiance spectra shown in Fig. 2 were obtained.[3,4] The data in Figs. 1 and 2, displayed in colorimetric form by Fig. 3, exhibit many intricate and beautiful phenomena which are manifestations of some of the physical principles discussed in this paper.

The importance of light in the sea is apparent when it is recalled that solar radiation supplies most of the energy input to the ocean and supports its ecology

* Most of the investigations described in this paper were supported by the Office of Naval Research and the Bureau of Ships of the U. S. Navy. Grants from the National Science Foundation have also aided the work. At certain times in the past the research was supported by the National Defense Research Committee and by the U. S. Navy's Bureau of Aeronautics.

[1] See E. F. DuPré and L. H. Dawson, "Transmission of Light in Water: An Annotated Bibliography," U. S. Naval Research Laboratory Bibliography No. 20, April, 1961 for abstracts of 650 publications by over 400 authors in more than 150 Swiss, German, French, Italian, English, and U. S. journals and other sources from 1818 to 1959.

[2] S. Q. Duntley, *Visibility Studies and Some Applications in the Field of Camouflage*, Summary Tech. Rept. of Division 16, NDRC (Columbia University Press, 1946), Vol. II, Chap. 5, p. 212.

[3] See J. G. Moore, Phil. Trans. Roy. Soc. (London) **A240**, 163(1946–48) for a method of using such data to determine depth and attenuation coefficients of shallow water.

[4] See G. A. Stamm and R. A. Hengel, J. Opt. Soc. Am. **51**, 1090 (1961) for data on the spectral *irradiance* incident on the underside of an aircraft flying above the ocean.

through photosynthesis. The biological productivity of an acre of ocean has been estimated to be, on a world-wide average, comparable to that of an acre of land. Most of the surface of our "water planet" is covered by seas and its atmosphere contains great quantities of water in the form of vapor and clouds. Light in the sea enables the native inhabitants of the water world to find their food and to evade attack. Nowhere in nature is protective coloration more perfectly or dramatically displayed than in the feeding grounds of the sea. Man and his cameras may view underwater scenes by means of daylight or with the aid of artificial lighting devices. Many biological organisms, including some living at very great depth, produce their own light at or near the wavelength for which water is most transparent, presumably both for vision and for signaling. All of these

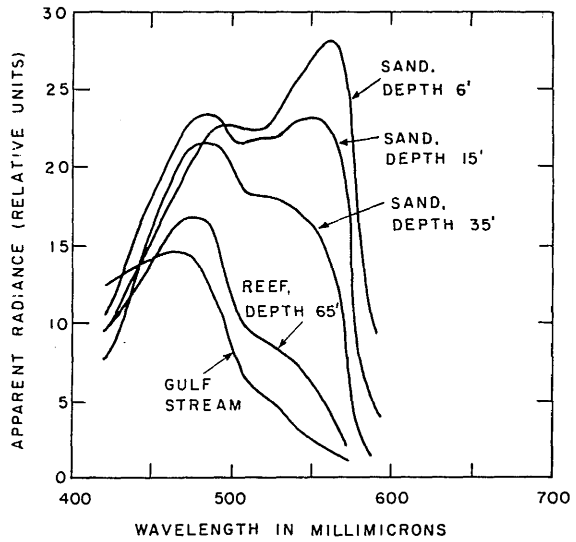

FIG. 1. Spectroradiometric curves of light from the nadir reaching a spectrograph mounted in a glass-bottomed boat over shoals off Dania, Florida (March 1944). Spectral resolution: 7.7 mμ; spatial resolution: 2.0×10^{-6} sr.

aspects of light in the sea can be treated by describing the optical nature of ocean water, the distribution of flux diverging from localized underwater light sources, the propagation of highly collimated beams of light, and the penetration of daylight into the sea. An integrated account of these topics is the subject of this paper.

OPTICAL NATURE OF OCEAN WATER

Most of the optical properties of ocean water as well as many of the principles which govern the propagation of light in the sea can be studied by injecting a highly collimated beam of monochromatic light into otherwise unlighted water and measuring all aspects of the resulting distribution of flux. This investigative approach even provides a basis for understanding the distribution of daylight in the sea and the submarine lighting pro-

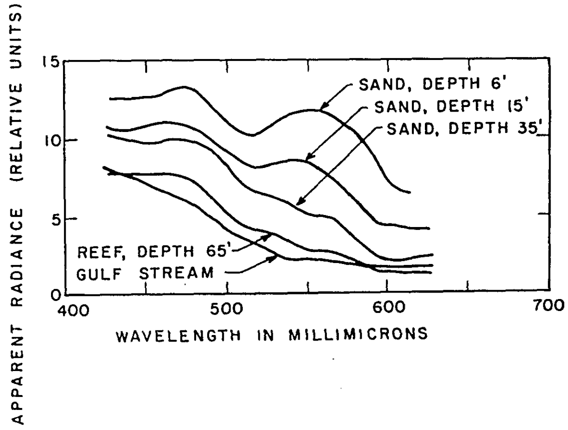

FIG. 2. Spectroradiometric curves of light from the nadir reaching a spectrograph in an airplane 4300 ft above the same ocean locations as in Fig. 1. Spectral resolution: 7.0 mμ; spatial resolution: 3.2×10^{-6} sr.

duced by artificial underwater light sources, for any optical input to the water may be represented by an appropriate superposition of highly collimated, monochromatic beams. The following paragraphs describe a variety of experiments which have been made by using a collimated, underwater light source, shown schematically in Fig. 4, at the Visibility Laboratory's Field Station at Diamond Island, Lake Winnipesaukee, New Hampshire.

Attenuation of a Collimated Beam

If a collimated beam of monochromatic light is injected into macroscopically homogeneous water by

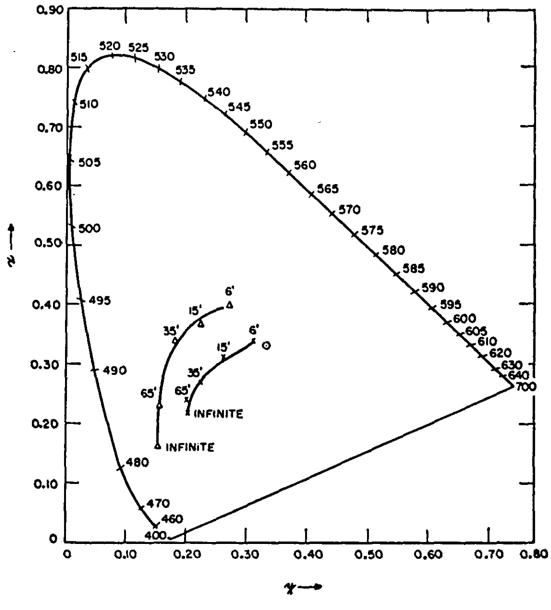

FIG. 3. CIE chromaticity diagram showing loci of the colors of ocean shoals as seen from an altitude of 4300 ft (shorter curve) and from a glass-bottomed boat (longer, upper curve). The points were calculated from the spectral radiance data in Figs. 1 and 2. The circled point represents CIE source C.

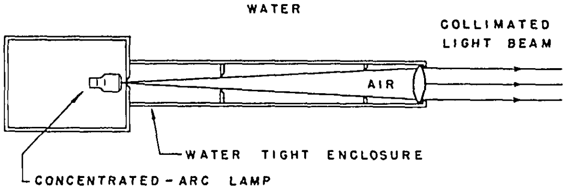

FIG. 4. Schematic diagram of the highly collimated underwater light source represented by a cross-hatched block in Figs. 5, 6, 7, 13, 20, and 21. This source was used in obtaining part or all of the data presented in Figs. 9, 10, 12, 17, 18, 20, and 22. Interchangeable 2, 10, 25, and 100 w zirconium concentrated-arc lamps in a water-tight air-filled enclosure produce nominal total beam spreads of 0.010°, 0.046°, 0.085°, and 0.174°, respectively, when used with a Wratten No. 61 green filter and a specially constructed air-to-water collimator lens having an effective first focal length of 495 mm. This lens, designed for the author by Justin J. Rennilson, is a cemented doublet 55 mm in diameter having radii $r_1=269.75$ mm, $r_2=r_3=102.60$ mm, $r_4=-325.0$ mm and axial thicknesses $t_1=3.0\pm0.2$ mm, $t_2=6.5\pm0.2$ mm. The first element is of Hayward LF-2 glass ($N_D=1.5800\pm0.0010$; $\nu=41.0$) and the second is of Hayward BSC-1 ($N_D=1.5110\pm0.0010$; $\nu=63.5$). The free aperture is 50.0 mm. The first back focal length of the doublet with its last surface in water is 493.88 mm. The air–glass surface was treated for increased light transmission. The achromatization is such that with the 2-W concentrated-arc lamp the extreme ray divergence is 0.0031°, 0.0039°, and 0.0109° at 480, 520, and 589 mμ, respectively, when the lamp is used in fresh water having a temperature of 20°C. A Wratten No. 61 green filter was used during all of the experiments with this lamp, but it does not appear in Fig. 4 because it was always incorporated in the photometer or the camera. An external circular stop (not shown) can be mounted in the water close to the lens whenever a smaller beam diameter is desired.

means of an underwater projector, as suggested by Fig. 5, it is found that the residual radiant power P_r^0 reaching a distance r *without having been deviated by any type of scattering process* is

$$P_r^0=P_0e^{-\alpha r}, \tag{1}$$

where P_0 represents the total flux content of the beam as it leaves the projector. The zero superscript on P_r^0 denotes the *zero scattering order*, i.e., nonscattered radiant power. The *spectral volume attenuation coefficient* α, defined by Eq. (1), has the dimension of reciprocal length and can be expressed in *natural log units per meter* (ln/m), natural log units per foot (ln/ft), etc; it is a scalar point function of position which may vary along any underwater path of sight if the water is macroscopically nonhomogeneous.

The attenuation of a beam of light by water results from two independent mechanisms: *scattering* and *absorption.* Scattering refers to any random process by which the *direction* of individual photons is changed without any other alteration. Absorption includes all of the many thermodynamically irreversible processes by which photons are changed in their nature or by which the energy they represent is transformed into thermal kinetic energy, chemical potential energy, and so on. Transformation of photon energy into thermal kinetic

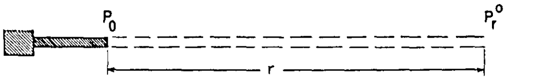

FIG. 5. Illustrating the geometry of Eq. (1). The cross-hatched block represents the collimated underwater light source (projector) shown schematically in Fig. 4.

energy of the water is the major absorption mechanism in the ocean. Photosynthetic conversion of light into chemical potential energy is, of course, measurable and vital to the existence of life in the sea. Visible light fluorescence and transpectral effects are ordinarily too minute to be detected in ocean water. The volume attenuation coefficient α is the sum of the *volume absorption coefficient* a and the *total volume scattering coefficient* s: thus $\alpha=a+s$.

Wavelength dependence. The attenuation coefficient of all water (pure, distilled, or natural) varies markedly with wavelength. Typical data are summarized in Table I, wherein the reciprocal of the volume attenuation coefficient, called *attenuation length,* has been tabulated rather than attenuation coefficient for three reasons: (1) a distance is easier to visualize and to remember than a reciprocal distance; (2) visibility calculations and many experiments by swimmers show that any large dark object (such as a dark-suited swimming companion) is just visible at a horizontal distance of about 4 attenuation lengths when there is sufficient underwater daylight; (3) many physicists like to characterize any absorbing–scattering medium (such as water) by the mean free path for a photon in the ordinary kinetic theory sense; this is the attenuation length $1/\alpha$. The term, "20-meter water," signifying water having an attenuation length of 20 m/ln, facilitates verbal discussions.

TABLE I. Attenuation length of distilled water at various wavelengths.[a–c]

Wavelength mμ	Attenuation length ($1/\alpha$) meters/ln
400	13.
440	22.
480	28.
520	25.
560	19.
600	5.1
650	3.3
700	1.7

[a] E. O. Hulburt, J. Opt. Soc. Am. 35, 698 (1945).
[b] For ultraviolet attenuation data see L. H. Dawson and E. O. Hulburt, J. Opt. Soc. Am. 24, 175 (1934).
[c] For near infrared attenuation data see J. A. Curcio and C. C. Petty, J. Opt. Soc. Am. 41, 302 (1951).

Water possesses only a single important window, the peak of which lies near 480 mμ unless it is shifted toward the green by dissolved yellow substances. Such yellow solutes, usually prominent in coastal waters, consist of humic acids, melanoidins, and other compounds which result from the decomposition of plant and animal materials. Clear ocean water is so selective in its absorption that only a comparatively narrow band of blue-green light penetrates deeply into the sea[5] (see Fig. 1) but this radiation has been detected at depths greater than 600 m with a multiplier phototube photometer.[6]

[5] J. E. Tyler, Limnology and Oceanography 4, 102 (1959).
[6] S. Q. Duntley, Natl. Acad. Sci.—Natl. Research Council Publ. 473, 79 (1956).

Many have wondered whether there exists any fine structure in the volume attenuation function which was beyond the spectral resolution available to the investigators whose results are summarized by Table I. Is there, for example, a narrow-band window of high transmission? It is the concensus of most physicists that the atomic and molecular structures involved in water provide no reason to expect any significant fine structure in the spectral attenuation function. A careful spectroscopic examination of the region from 3750 to 6850 Å with a resolution of 0.2 Å and sensitivity sufficient to detect a variation of 0.02 ln/m in the attenuation coefficient has been reported by Drummeter and Knestrick.[7] They detected no fine structure, i.e., no narrow-band window.

Water Clarity

The clearest body of ocean water of large extent is reputed to be in the Sargasso Sea, a vast region of the Atlantic Ocean east of Bermuda. Jerlov has reported very clear water between Madeira and Gibraltar,[8] as

TABLE II. Attenuation length of the Atlantic Ocean for wavelength 465 mμ at various depths in the vicinity of Madeira and Gibraltar.[a]

Depth meters	Attenuation length ($1/\alpha$) meters/ln
0–10	19
10–25	20
25–50	18
50–75	15
75–90	16

[a] N. G. Jerlov, Kgl. Vetenskap. Vitterh. Handl. F.6, Ser. B, BD8.N:o11 (1961).

summarized by Table II. Although clearer water was found at 10 m depth than at 90 m at this location, the reverse is often true elsewhere. Optical oceanographic data are not numerous. Jerlov's measurements during the Swedish Deep Sea Expedition of 1947–48 are classical examples. Table III shows some of these data selected to typify certain indicated locations.[9]

DuPré and Dawson[1] give many references to water-clarity data; users of published data should note carefully whether the attenuation coefficients reported are expressed in ln/m or in log/m and whether the values refer to the attenuation coefficient α for nonscattered light, as in a collimated beam, or to some form of *diffuse attenuation coefficient* K, discussed later in this paper. No single number can adequately specify the clarity of any natural water because two independent mechanisms, absorption and scattering, govern water

TABLE III. Attenuation length of ocean water for wavelength 440 mμ at various locations.[a]

Location	Attenuation length ($1/\alpha$) meters/ln
Caribbean	8
Pacific N. Equatorial Current	12
Pacific Countercurrent	12
Pacific Equatorial Divergence	10
Pacific S. Equatorial Current	9
Gulf of Panama	6
Galapagos Islands	4

[a] N. G. Jerlov, Reports of the Swedish Deep Sea Expedition of 1947–48 (1951), Vol. 3, p. 49, Table 27.

clarity. Even for monochromatic light, at least two coefficients, such as α and K, are required, and a more complete specification requires data on the volume scattering function $\sigma(\vartheta)$, defined in the paragraphs which follow.

Daylight, abundant in the mixed layer near the surface, supports the growth of phytoplankton in the biologically productive regions of the oceans. These, in turn, feed a zooplankton population. The transparent planktonic organisms, ranging in size from microns to centimeters, scatter light and thereby produce optical attenuation. Settling of the plankton, particularly after death, tends to produce a high concentration of these scatters just above the thermocline which ordinarily exists at the lower boundary of the mixed layer in the sea.[10] Below the thermocline lies clearer water which may be optically uniform for tens or hundreds of meters before some different water mass is encountered. Interestingly, the optical structure of the ocean resembles, in a sense, that of the atmosphere if depth is considered as analogous to altitude and a proper allowance is made for the decrease of atmospheric density with height.

Scattering

Scattering of light in the sea is predominantly due to transparent biological organisms and particles large compared with the wavelength of light. The magnitude of the scattering is, therefore, virtually independent of wavelength.[11] The variation of attenuation length with

[7] L. F. Drummeter and G. L. Knestrick, U. S. Naval Research Laboratory Rept. No. 5642 (1961).
[8] N. G. Jerlov, Kgl. Vetenskap. Vitterh. Handl. F.6, Ser. B, BD8. N:o 11 (1961).
[9] N. G. Jerlov, Reports of the Swedish Deep Sea Expedition of 1947–48 (1951), Vol. III, p. 49, Table 27.

[10] Multiple thermoclines often form in the upper portion of the sea; the maximum optical attenuation is associated with the maximum vertical temperature gradient and frequently falls on a secondary thermocline. Internal waves shift the scattering layer vertically. See E. C. La Fond, E. G. Barnham, and W. H. Armstrong, U. S. Navy Electronics Laboratory Rept. 1052 (July 1961), p. 15. Also see J. Joseph, Deut. Hydrograph. Z., Nr. 5 (1961).
[11] Scattering is also contributed by fine particles, by molecules of water, and by various solutes, but these contributions are usually quite minor and often difficult to detect. Even in very clear, blue ocean water scattering by water molecules produces only 7% of the total scattering coefficient and is dominant only at scattering angles near 90°, where it provides more than 2/3 of the scattered intensity (see reference 8); although the magnitude of this small component of scattering varies inversely as the fourth power of wavelength (λ^{-4}), it is so heavily masked by nonselective scattering due to large particles that total scattering in the sea is virtually independent of wavelength. The prominent blue color of clear ocean water, apart from sky reflection, is due almost entirely to selective absorption by water molecules.

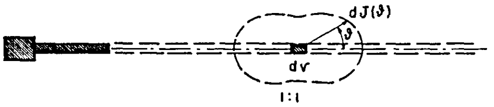

FIG. 6. Polar diagram illustrating Rayleigh scattering by pure water. The ratio of the light scattered into the rear hemisphere to that scattered into the forward hemisphere is 1 to 1. The cross-hatched block represents the collimated underwater light source shown schematically in Fig. 4.

wavelength (see Table I) is due almost wholly to selective absorption.

In the blue region of the spectrum, centering at 480 mμ, approximately 60% of the attenuation coefficient of clear, blue ocean water is due to scattering and 40% is due to absorption; e.g., $s=0.030$ ln/m and $a=0.020$ ln/m.[8] In all other spectral regions absorption is overwhelmingly predominant in very clear water.

Since scattering is virtually independent of wavelength its detailed nature is best revealed by means of experiments conducted at or near the wavelength of minimum absorption. This means experiments with blue light in clear, blue ocean water and experiments with green light in greenish coastal and lake waters.

Scattering by pure water. Consider a scattering experiment performed in pure water, that is, in water molecules containing no dissolved or particulate matter whatsoever. As in Fig. 6, consider an element of volume dv receiving collimated, nonpolarized, monochromatic irradiance H to act as source of scattered light, producing radiant intensity $dJ(\vartheta)$ at scattering angle ϑ. Scattering by the water molecules will be Rayleighian, with $dJ(\vartheta)\sim\lambda^{-4}$ and with the shape of the intensity function $dJ(\vartheta)$ characterized by $(1+0.835\cos^2\vartheta)$ (see reference 12). Since even the most elaborately prepared distilled water samples show particulate matter when examined in a light beam, scattering by truly pure water has probably never been measured.

Scattering by distilled water. A colleague, John E. Tyler, has performed scattering experiments in many samples of commercial distilled water[13]; Fig. 7 shows a typical result. Obviously, the scattering produced by this sample of distilled water is very different from that predicted for pure water. The predominant forward scattering is caused by a comparatively few large particles. The dotted curve may be regarded either as a polar plot of the radiant intensity $dJ(\vartheta)$ or of the *volume scattering function* $\sigma(\vartheta)$, defined by the equation $dJ(\vartheta)=\sigma(\vartheta)\,H dv$, where H is the irradiance produced by the collimated lamp on the volume dv. The dimension of $\sigma(\vartheta)$ is reciprocal length; typical units are reciprocal steradian-meters or reciprocal steradian-feet. The polar curve in Fig. 7 is not complete; it begins at $\vartheta=22\ 1/2°$ and stops at $\vartheta=165°$. All conventional scattering meters designed to be used *in situ* possess the limitation that they cannot measure scattering at small angles. Fortunately, the total scattering coefficient s, defined by the relation

$$s=2\pi\int_0^{\pi}\sigma(\vartheta)\sin\vartheta d\vartheta,$$

is insensitive to the magnitude of small-angle forward scattering. Unfortunately, however, the propagation of highly collimated light does depend importantly on small-angle scattering.

Small-angle scattering. The author has devised a special (coaxial) *in situ* scattering meter to supply the missing forward part of the curve. Figure 8 is a schematic diagram of the instrument. It shows the optical system adjusted to measure the volume scattering function at a scattering angle of 1/2 deg. Such a datum was obtained with the coaxial scattering meter at the Diamond Island Field Station and determines the upper end of the upper curve in Fig. 9. This may be the first *in situ* measurement of small-angle scattering by natural water. The very large scattering found at small scattering angles is believed to have been caused primarily by re-

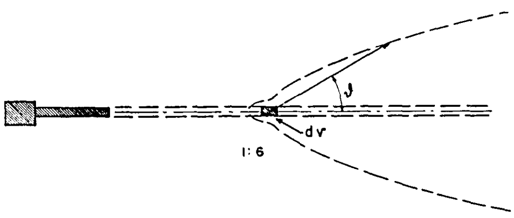

FIG. 7. Polar diagram illustrating measured scattering by a typical sample of commercial distilled water. The ratio of the light scattered into the rear hemisphere to that scattered into the forward hemisphere is 1 to 6 for this water sample. Data are by Tyler (see reference 13). The scale of this polar plot is smaller than that used in Fig. 6.

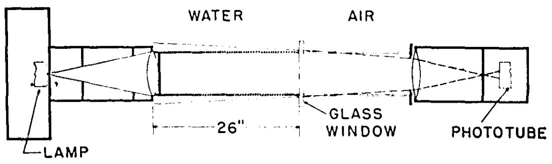

FIG. 8. Coaxial scattering meter for *in situ* measurement of the volume scattering function at small scattering angles. In this schematic drawing the vertical scale has been exaggerated five times over the horizontal scale in order to illustrate the principle of the device more clearly. The collimated underwater light source shown in Fig. 4 is used with the addition of an external opaque central stop which results in the formation of a thin-walled hollow cylinder of light. This traverses 26 in. of water to a high-quality glass window behind which, in air, is a photoelectric telephotometer with a 2° total field of view. The light source and the telephotometer are coaxial, but the latter is equipped with an external stop small enough to exclude the hollow cylinder of light so that only light scattered by the water is collected. The cylindrical scattering volume is indicated by cross-hatching. The upper limit of the scattering angle is determined by the field of the telephotometer and the lower limit is set by the size of its external stop, i.e., by the entrance pupil. A detailed geometrical analysis of the configuration depicted above shows that the scattering is measured at 0.47 deg±0.15°; this datum is used as the volume scattering function for 1/2° scattering angle in Figs. 9 and 10. Photometric calibration of the scattering meter is achieved by removing the external stop on the telephotometer.

---

[12] L. H. Dawson and E. O. Hulburt, J. Opt. Soc. Am. 31, 554 (1941).

[13] J. E. Tyler, Limnology and Oceanography 6, 451 (1961).

fractive deviations produced by the passage of the collimated light beam through transparent plankton having an index of refraction close to that of water. The curve shape at small scattering angles is chosen to suggest that the magnitude of the volume scattering function may merge tangentially with that of the irradiating beam at vanishingly small angles.

Chemists have, for many years, made laboratory measurements of very small-angle scattering from tiny volumes of scattering materials.[14] Koslyaninov[15] has reported volume scattering measurements at angles down to 1 deg by means of a shipboard laboratory apparatus using water samples brought on board for measurement. Figure 10 shows the data of Koslyaninov for the East China Sea superimposed upon the lake data from Fig. 9 after normalization at a scattering angle of 90°, as denoted by the small circle in the figure. The forward-scattering portions of the curves are similar in shape.

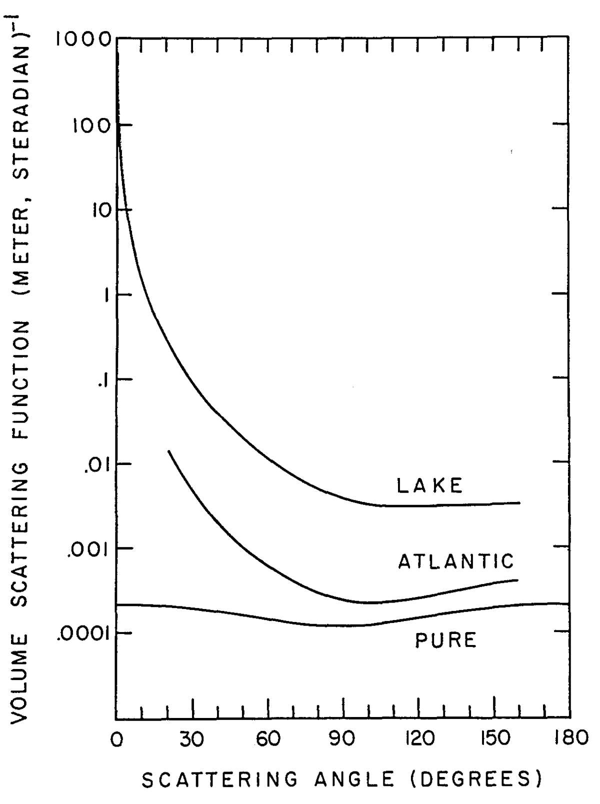

FIG. 9. Volume scattering function curves for pure water (Dawson and Hulburt, see reference 12), the Atlantic between Madeira and Gibraltar (Jerlov, see reference 8), and the Diamond Island Field Station, Lake Winnipesaukee, New Hampshire. The upper curve (lake) represents *in situ* measurements at 5° intervals between scattering angles $20° > \vartheta > 160°$ by means of a conventional type, pivoted-arm scattering meter and a single datum at $\vartheta = 0.5°$ obtained *in situ* with the coaxial scattering meter shown schematically in Fig. 8; the data are of 20 August 1961; and are for green light isolated by means of a Wratten No. 61 filter.

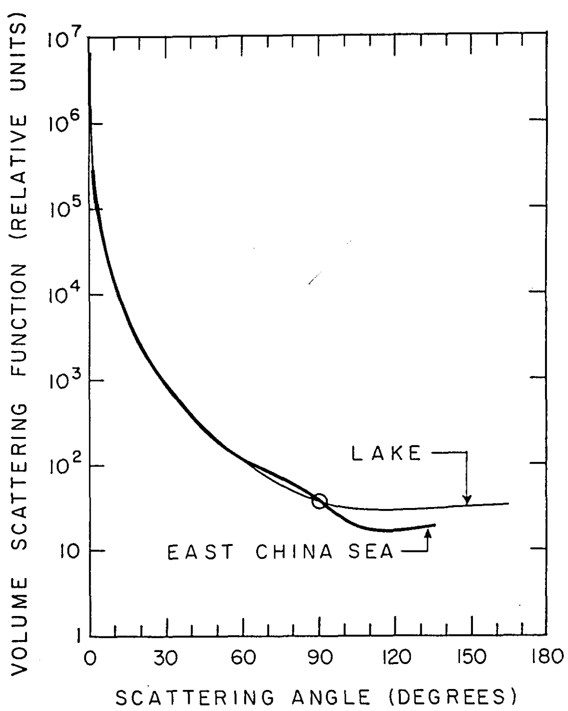

FIG. 10. Comparison of the shape of the *in situ* volume scattering function data for Lake Winnipesaukee, New Hampshire, from Fig. 9 with the shape of a curve representing the *in vivo* scattering data obtained by Koslyaninov (see reference 15) using a shipboard laboratory apparatus and a sample of water taken from the East China Sea. The curves have been normalized at a scattering angle of 90° (circled point) for purposes of shape comparison. Koslyaninov used blue light isolated by means of an absorption filter having an effective wavelength of 494 mμ; he reported data at scattering angles of 1, 2.5, 4, 6, 10, 15, 30, 50, 70, 110, and 144 deg. The curves are similar in shape for scattering angles less than 60°.

Comparison with distilled water. Figure 11 shows a comparison of *in situ* scattering measurements by Tyler[13] of commercial distilled water and clear Pacific water. Ocean water scatters more light than does distilled water but the similarity of the shape of the curves is striking and interesting in its implication of the predominant role of large particle scattering.

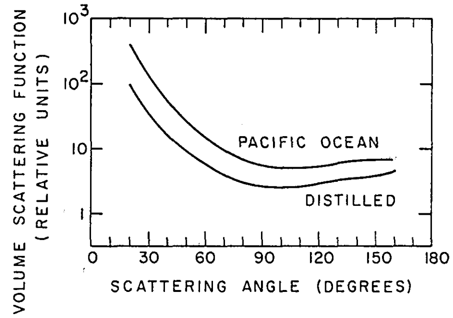

FIG. 11. Comparison of *in situ* scattering data by Tyler (see reference 13) in clear Pacific ocean water near Catalina with comparable data for a typical sample of commercial distilled water. Both curves were obtained with the same pivoted-arm scattering meter and are in the same relative units. The data are for green light isolated by means of a Wratten No. 61 filter.

[14] H. F. Aughey and F. J. Baum, J. Opt. Soc. Am. 44, 833 (1954).
[15] M. V. Koslyaninov, Trudy Inst. Okeanol. Acad. Nauk S.S.S.R. **25**, 134 (1957).

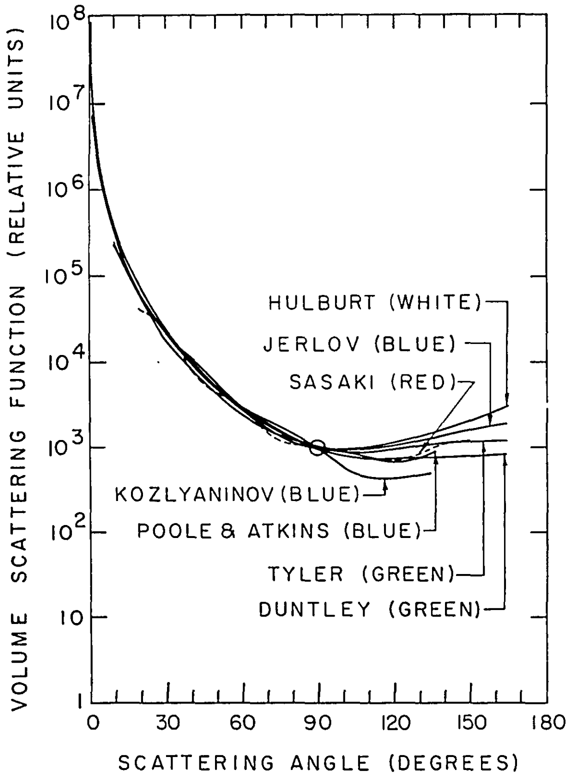

FIG. 12. Comparison of scattering data by seven investigators using dissimilar instruments in seven different parts of the world. All curves are superimposed at a scattering angle of 90°, as indicated by the circled point. Gross similarity in curve shape is apparent in the forward ($0<\vartheta<90°$) scattering directions despite major differences in water clarity (2 m/ln$<1/\alpha<20$ m/ln), spectral region, geographical location, instrumental design, and experimental technique. Most of the scattering in natural waters is caused by transparent organisms and particles large compared with the wavelength of light. The scattering is believed to result chiefly from refraction and reflection at the surfaces of these scatterers. As a consequence, scattering at small forward angles predominates and polarized light tends to preserve its polarization. To the extent that all scattering curves have identical shapes the scattering by natural waters can be specified in terms of some single number, such as the total volume scattering coefficient s or the volume scattering function at some selected angle.

Comparison between natural waters. A comparison of the scattering properties of natural waters is afforded by Fig. 12, which shows a superposition of measurements by seven different investigators using seven dissimilar instruments in seven different parts of the world. Three of the measurements were made with blue light, two were made with green light, the dashed curve was obtained with red light, and one investigator employed white light. The attenuation lengths of the waters ranged 2 m/ln for the author's lake data to 20 m/ln in the case of Jerlov's data for the Atlantic. It appears that the shape of the forward portion of the volume scattering function is remarkably similar in all of these natural waters, but that significant differences occur in the character of the backscattering they produce.

Although it is a useful first-order concept that natural waters are somewhat similar in the shape of their volume scattering functions, it is important to note therefore that measurable differences apparently exist and that ocean water masses might therefore be identified by their scattering function curves.

Multiple scattering. The propagation of light in the sea is complicated by multiple scattering. Consider, as in Fig. 13, a plane surface irradiated at normal incidence by the collimated lamp shown in Fig. 4. Every point on the plane receives scattered light from every volume element within the light beam. It receives, moreover, multiply scattered light from every elementary volume of water near the beam. In fact, every volume element within the sea is irradiated by every other volume element both inside and outside the beam. The figure illustrates how irradiation is produced throughout the plane by second-, third-, and fourth-order scattering.

Although theoretical treatments of the effects of multiple scattering on the distribution of light in the sea both from underwater sources and from daylight have been undertaken with partial success by several workers, no fully practical solution has yet been evolved. Some derivations include only secondary scattering and neglect higher-order effects. Others, following the practice of neutron physics, assume the scattering to be virtually isotropic, that is to say, the shape of the volume scattering function is assumed to be spherical or nearly so; this is, of course, highly unrealistic. Four patterns of approach characterize the theories: (1) *Multiple integration* using the volume scattering function, the attenuation coefficient α, and the inverse square law; these treatments suffer from complexity, are never complete, and may neglect sizeable components of flux but some useful approximate solutions have been achieved in special cases. (2) *Diffusion theory.* This applies rigorously only to isotropic or very mildly nonisotropic scattering systems which are not found in the sea; nevertheless, considerable success has been achieved in the prediction of *irradiance* at long ranges; diffusion theory is, however, unable to yield much information concerning the directional characteristics of the underwater light field. (3) *Radiative transfer.* This method is based upon equations of transfer, sometimes in vector form; these integro-differential equations are solved in practice by iterative procedures on the largest electronic computers. (4) *Monte Carlo procedures.* These also require the use of large electronic computers. Al-

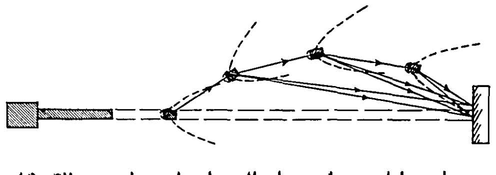

FIG. 13. Illustrating the irradiation of an object by multiply scattered light at arbitrary points inside and outside the light beam. The dotted curve associated with each cross-hatched volume element has the shape shown in Fig. 7 and represents a polar plot of the volume scattering function. The need for additional scattering data at small forward angles is obvious.

though, *in principle*, either of the two latter approaches appears to be capable of handling all underwater light propagation problems, neither has thus far achieved appreciable practical success in the treatment of point source or collimated beam geometrics, for the calculations are too massive for even the largest of electronic computers. Success has, however, been achieved for the case of daylight in the sea,[16] wherein the development of theory and the evolution of practical computation procedures followed quickly after experimental explorations of underwater daylight radiance distributions had produced a body of data, described later in this paper, from which valid assumptions could be made and against which predictions could be checked. This experience prompted the author to begin a program of experimental explorations of the distribution of light produced by submerged divergent light sources and by collimated lamps underwater. These explorations are still in progress, but some of the conclusions reached thus far are summarized in the following section.

DIVERGENT LIGHT IN THE SEA

Marine organisms which emit nearly hemispherical flashes of light are found at virtually all depths in the sea. Underwater lighting for vision, television, or photography is often accomplished by means of incandescent lamps or flash tubes which approximate point sources and emit divergent flux. Quantitative prediction of the irradiation produced by such lamps at the object, on its background, and throughout the observer's path of sight can enable optimum lighting arrangements and camera positions to be planned in advance and exposure to be predicted with sufficient accuracy to permit high-contrast photographic techniques to be employed effectively.

Apparent Radiance at the Object

Every underwater object and every elementary volume of water irradiated by a submerged divergent light source is lighted by an apparent radiance distribution which depends upon the radiant intensity distribution of the lamp, the optical properties of the water, and the lamp distance. This radiance distribution can be seen, photographed, and measured by an observer stationed at the position of the object. To such an observer a receding, uniform, spherical lamp appears to be surrounded by a glow of scattered light which becomes proportionately more prominent as lamp distance is increased, until at some range, often 18 to 20 attenuation lengths, the lamp image can no longer be discerned and only the glow is visible. The glow, however, may be seen for a considerably greater distance, depending upon the radiant intensity of the source and the ambient level of light in the sea.

Apparent radiance of the lamp. Densitometric meas-

[16] W. H. Richardson and R. W. Preisendorfer, Scripps Inst. Oceanog., Ref. 60-43 (1960).

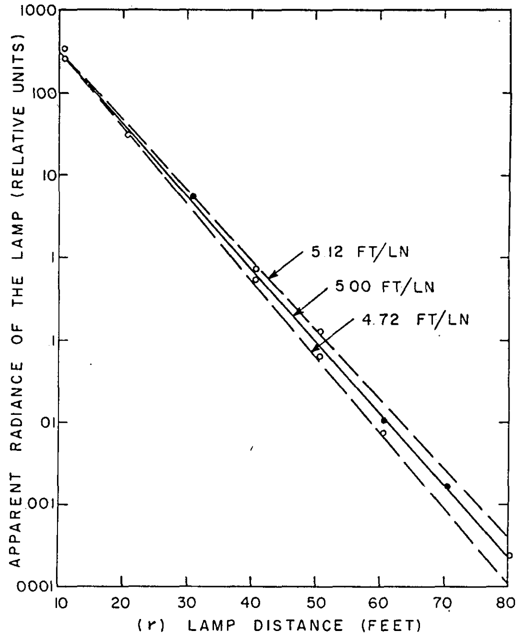

FIG. 14. Apparent radiance of a uniform, spherical underwater lamp at various distances, illustrating the exponential nature of the attenuation of apparent lamp radiance with distance. Photographic photometry was employed using a Wratten No. 61 filter and Eastman Plus X 35-mm film (Emulsion No. 5061-64-16A) developed to unity gamma in D-76. Exposure time at $f/1.5$ varied from 1.75 msec at a lamp distance of 10.5 ft to 180 000 msec when the lamp was 80 ft from the camera. The source of light was a 1000-W incandescent "diving lamp" (No. MG25/1) manufactured by the General Electric Company. The 3-in. spherical lamp envelope was sprayed with a white gloss lacquer in order to produce a uniform translucent white covering which gave the lamp the same radiant intensity in all directions (to within $\pm 7\%$) except toward the base, which was turned away from the camera. Two or more exposure times differing by 5- or 10-fold were used at each lamp distance. Open circles represent data from a single time of exposure; solid points indicate that identical values of apparent radiance were obtained from negatives made with two different exposure times. A solid straight line, representing an attenuation length $1/\alpha = 5.00$ ft/ln, has been drawn near the points. Dashed lines corresponding to attenuation lengths of 4.72 ft/ln and 5.12 ft/ln, respectively, represent values measured by means of a light-beam transmissometer before and after the all-night experimental session. Cooling of the water during the night correlated with the observed increase of attenuation length, presumably due to plankton shrinkage. Data are of 26 August 1959 at Diamond Island Field Station.

urements of the lamp images in a series of photographs of a receding spherical underwater light source produced the results shown in Fig. 14, wherein the close fit of the data to the solid straight line shows that the apparent radiance of the lamp is attenuated exponentially, as the equation

$$N_r = N_0 e^{-\alpha r}, \tag{2}$$

where N_r is the apparent radiance at distance r, N_0 is the inherent radiance of the lamp surface, and α is the attenuation coefficient for apparent radiance. The dashed lines, constructed from data secured with a light-beam transmissometer designed to conform with the requirements of Eq. (1), provide evidence that numerically identical attenuation coefficients α apply in

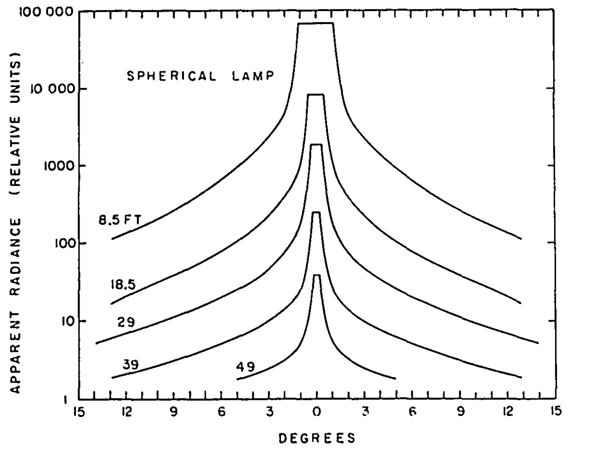

FIG. 15. Angular distribution of apparent radiance produced by a uniform, spherical, underwater lamp at distances of 8.5, 18.5, 29, and 39 feet. The lamp was identical to the one described in connection with Fig. 14. The photometry was by means of an automatic scanning, photoelectric, telephotometer having a circular acceptance cone 0.25° in diameter and with its spectral response limited by a Wratten No. 61 filter. Attenuation length was 5.1 ft/ln. Data are of 3 August 1961 at the Diamond Island Field Station.

Eqs. (1) and (2), indicating thereby that images are formed by photons transmitted without being scattered and that the contribution of scattered light to the exposure of the image portion of the negative was negligible.

Apparent radiance of the glow. Distributions of the apparent radiance of the glow surrounding the distant lamp were obtained by densitometry of the same series of photographs, but more accurate results have been achieved by means of an automatic scanning photoelectric telephotometer which was more free from stray light than was the camera. Distributions of apparent radiance as measured photoelectrically from the target position are shown in Fig. 15. The irradiance on any surface of the target facing the lamp can be computed from these curves and, if the reflectance and gloss characteristics of the target surfaces are known, the inherent radiance of the target in any specified direction can be calculated. If, moreover, the volume scattering function of the water and its attenuation length are known, calculations of inherent background radiance, path radiance, and apparent target contrast can be made from Fig. 15.

Irradiance at the Object

The surface of any underwater object is irradiated by (1) direct (nonscattered) light from the lamp and (2) scattered light. The *nonscattered* or *monopath irradiance* H_r^0 produced at normal incidence by a lamp radiant intensity J at distance r is given by the relation

$$H_r^0=Je^{-\alpha r}/r^2. \tag{3}$$

In addition to H_r^0, the object is irradiated by the scattered or *multipath irradiance* H_r^*. Thus the *total irradiance* $H_r=H_r^0+H_r^*$. Since H_r can be measured (see Fig. 16) and H_r^0 can be calculated by means of Eq. (3), H_r^* can be found by subtraction; thus, $H_r^*=H_r-H_r^0$.

Diffusion theory[17,18] based upon the assumption of isotropic scattering suggests that

$$H_r^*=JKe^{-Kr}/4\pi r, \tag{4}$$

where K is an attenuation coefficient for scattered light. If this K is given a value numerically equal to the attenuation function for daylight scalar irradiance k, as discussed later in the portion of this paper devoted to daylight in the sea, Eqs. (3) and (4), when summed, fit the data of Fig. 16 within experimental uncertainty both at short and at long lamp distances; between 10 ft (2 attenuation lengths) and 70 feet (14 attenuation lengths), however, the measured total irradiance is as much as twice the predicted values. A semiempirical modification of Eq. (4) which, added to Eq. (3), fits the data of Fig. 16 within experimental error is

$$H_r^*=2.5(1+7e^{-Kr})JKe^{-Kr}/4\pi r. \tag{5}$$

Effect of beam spread. Underwater sources of divergent light are seldom completely spherical in their radiant intensity distribution. Many underwater lamps

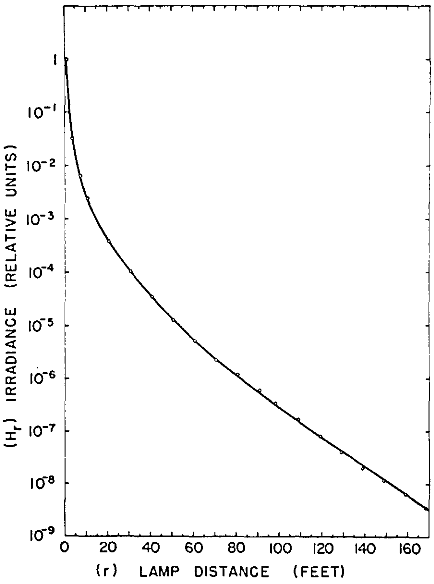

FIG. 16. Total irradiance produced at various distances by a uniform, spherical underwater lamp at the Diamond Island Field Station. The solid curve was passed through the data points by means of a least-squares procedure. The lamp was identical with the one described in connection with Fig. 14. The photometry was by means of an underwater photoelectric irradiance meter facing directly toward the lamp. The spectral response of the irradiometer was limited by means of a Wratten No. 61 green filter. The attenuation length of the water was 5.0 ft/ln. Data are of 26 August 1959.

[17] S. Glasstone and M. C. Edlund, *Elements of Nuclear Reactor Theory* (D. Van Nostrand and Company, Inc., Princeton, New Jersey, 1952), p. 107.

[18] R. W. Preisendorfer (private communication).

emit roughly conical patterns of flux 20° or more in total angular extent. Monopath irradiance is, of course, unaffected by the beam spread, and the effect on multipath irradiance is not large unless the lamp produces a highly collimated beam. Experiments with an underwater light source having a continuously variable beam spread down to 20° resulted in an empirical modification of Eq. (5) to the form

$$H_r^* = (2.5 - 1.5 \log_{10} 2\pi/\beta) \times [1 + 7(2\pi/\beta)^{1/2} e^{-Kr}] JKe^{-Kr}/4\pi r, \quad (6)$$

where β is the total beam spread. Equation (6) should not be used for beam spreads less than 20°.

Equations (4), (5), and (6) have been tested by the author only at the Diamond Island Field Station, but because of the similarity in the shape of the volume scattering functions of natural waters, as illustrated by Fig. 12, they may have nearly universal applicability as approximations for engineering purposes.

COLLIMATED LIGHT IN THE SEA

Underwater projectors producing beam spreads small compared with 1° exhibit distinctive properties. When seen from the position of the irradiated target, the head-on appearance of a distant, highly collimated lamp is remarkably similar to that of a broad-beam lamp at some lesser range. Thus, the bright disk-shaped image of the lamp is surrounded by a glow of scattered light, having an apparent radiance distribution like that shown in Fig. 17. Although it is difficult to distinguish a distant collimated lamp from a distant divergent source when each is observed from within its beam, radiance distribution measurements reveal subtle differences, the nature of which can be seen by comparing Figs. 15 and 17.

The appearance presented by a moderately distant, slightly averted collimated lamp is, however, very different from that of its divergent counterpart because the intense small-angle scattering, common to all natural waters, produces a readily visible, sharply defined, nearly cylindrical luminous column extending toward the observer from the collimated lamp. Near the lamp and on the axis of this column the monochromatic monopath irradiance normal to the beam at distance r is $H_r^0 = H_0 e^{-\alpha r}$, where the irradiance H_0 in the water at the lens of the projector is given by $H_0 = J\psi^2 D^{-2}$ in terms of radiant intensity J, total beam spread ψ, and diameter D of the light beam. Beyond the distance $r' = D/\psi$, at which the lens replaces the source as the aperture stop of the irradiating system, H_r^0 is given by

$$H_r^0 = Je^{-\alpha r}/r^2 = H_0 e^{-\alpha r}(D/\psi r)^2 = H_0 e^{-\alpha r}/(r/r')^2 \quad (7)$$

if diffraction is negligible.

The dashed lines in Fig. 18 illustrate the foregoing relations applied to the case of three collimated lamps having a divergence of 1/6° and exit pupil diameters of 1/300, 2/300, and 8/300 of an attenuation length,

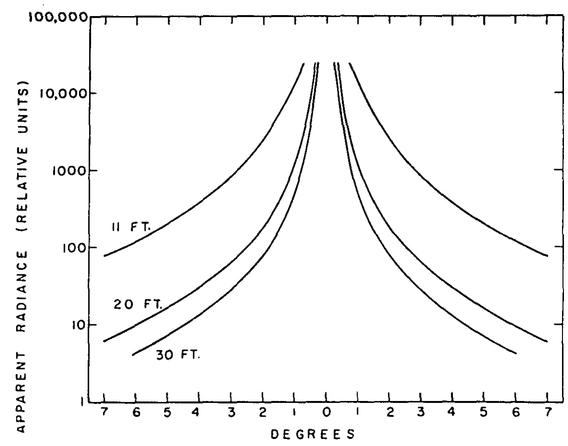

FIG. 17. Apparent radiance produced by scattering from the beam of the highly collimated underwater lamp shown in Fig. 4. The photometry was by means of an automatic scanning, photoelectric telephotometer having a circular acceptance cone 0.25° in diameter and with its spectral response limited by a Wratten No. 61 filter. The beam from the lamp had a divergence of 0.01°; it was directed toward the telephotometer and filled the entrance pupil of that instrument at all times. Lamp distances of 11, 20, and 30 ft were used. Tests of the telephotometer showed that the data in Fig. 17 are free from stray-light effects. Attenuation length of the water was 6.7 ft/ln. The data are of 11 August 1961 at the Diamond Island Field Station.

respectively. For these three lamps the distances r' are 1.15, 2.30, and 9.20 attenuation lengths. The points at $r = r'$, beyond which Eq. (7) applies, lie within the diagram for both of the two smaller lamps and are indicated by triangles. In all cases, diffraction will lower the dashed curves.

The total irradiance H_r on the axis of a collimated beam exceeds the monopath irradiance H_r^0 by the multipath contribution H_r^*; i.e., $H_r = H_r^0 + H_r^*$. This is illustrated by the experimental data points shown in Fig. 18 and the solid curves which have been fitted to them. In the case of the two smaller lamps the multipath contribution was not detected at ranges shorter than r', indicated by the triangle points, but this is not true in the beam from the large-diameter lamp where H_r^* and H_r^0 are approximately equal throughout much of the range of distances covered by the data. The steadily increasing separation of the solid and dashed curves in each of the lower pairs implies that multipath irradiance becomes dominant at large lamp distances.

Data such as those in Fig. 18 can be used to calculate the ratio of monopath to multipath irradiance; i.e., H_r^0/H_r^*. This ratio, independent of the intensity of the lamp or its radiant power output, is a measure of the beam content of the light; it is the ratio of image-forming light transmitted by the water path to the non-image-forming (scattered) light arriving at the irradiated object. Applications dependent on the retention of narrow-beam geometrical characteristics, of coherence, or of single-valued transmission time may require that some usable fraction of the irradiance consist of nonscattered (monopath) light. Figure 19 is a

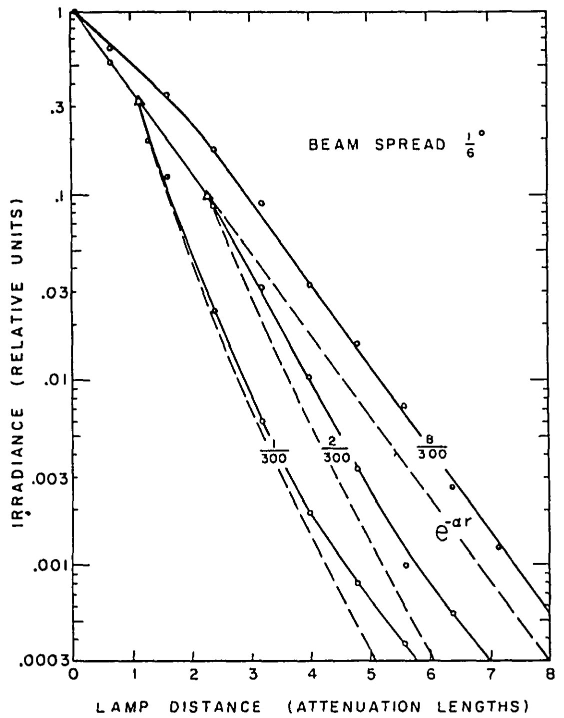

FIG. 18. Irradiance normal to the axis of the beam of light having a divergence of 1/6° produced by a collimated underwater lamp (Fig. 4) at distances up to 8 attenuation lengths is shown by the data points and the solid lines for beam diameters of 1/300, 2/300, and 8/300 of an attenuation length. The data are of 14 August 1961 at the Diamond Island Field Station; attenuation length $1/\alpha=6.3$ ft/ln. Dashed lines represent the monopath irradiance in each case computed from Eq. (7). Geometrical divergence reduces the axial monopath irradiance at all lamp distances beyond the points marked by triangles, which occur at 1.15 and 2.30 attenuation lengths for the two smaller lamps and at 9.20 attenuation lengths (not shown) for the largest lamp. Spreading of the beam by diffraction also reduces the monopath irradiance at all lamp distances, often dramatically. In a plot involving dimensionless lamp distance (such as Fig. 18), the dashed lines cannot be drawn to include the potentially major effect of diffraction because the wavelength of light is independent of the attenuation length, but they should be appropriately lowered when the figure is interpreted in terms of actual dimensions. The vertical separation between the dashed and the solid curves in each pair is a measure of the multipath irradiance. *Caution*: The data in this figure relate only to the axis of an aplanatic underwater projection system having a beam spread $\psi=1/6°$; they should *not* be scaled by the ratio D/ψ; they do *not*, for example, apply to the case of $\psi=1/60°$ and lamp diameters $D=1/3000$, 2/3000, or 8/3000 attenuation length.

plot of H_r^0/H_r^* for divergent sources. It shows that for a beam spread of 20°, $H_r^*=H_r^0$ at 1.4 attenuation lengths and that multipath irradiance predominates at large lamp distances. Experiments now in progress with light beams of small diameter and high collimation may produce corresponding curves for collimated lamps.

Irradiance near a highly collimated beam. All of the foregoing discussion has concerned irradiance produced on the axis of a collimated beam. Measurements of irradiance outside the light beam at various distances from the collimated lamp are shown in Fig. 20.

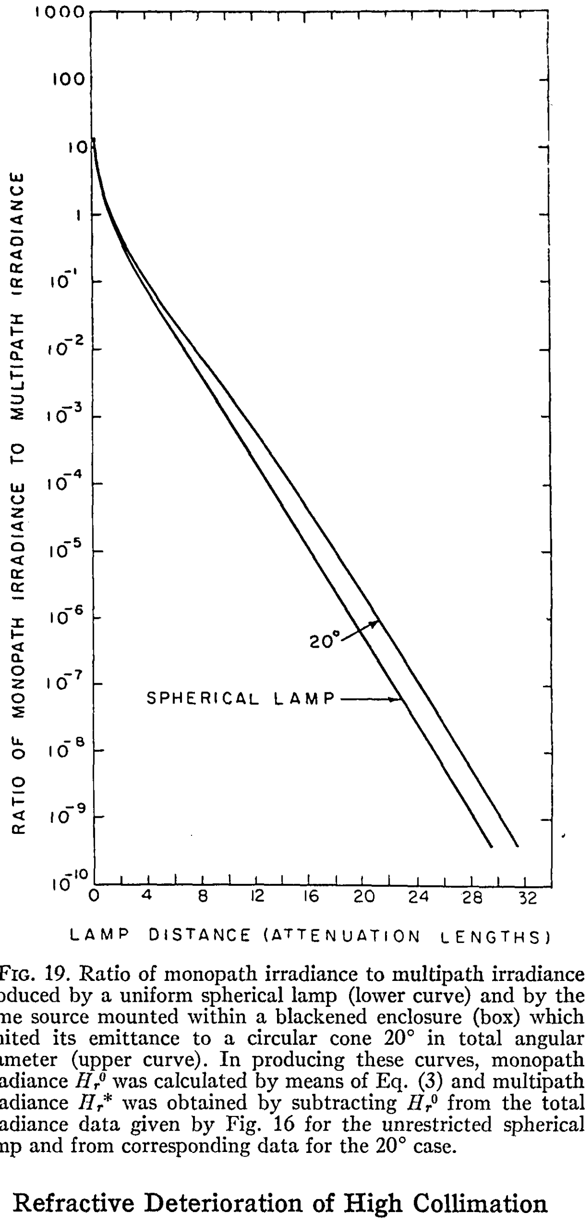

FIG. 19. Ratio of monopath irradiance to multipath irradiance produced by a uniform spherical lamp (lower curve) and by the same source mounted within a blackened enclosure (box) which limited its emittance to a circular cone 20° in total angular diameter (upper curve). In producing these curves, monopath irradiance H_r^0 was calculated by means of Eq. (3) and multipath irradiance H_r^* was obtained by subtracting H_r^0 from the total irradiance data given by Fig. 16 for the unrestricted spherical lamp and from corresponding data for the 20° case.

Refractive Deterioration of High Collimation

No discussion of the properties of highly collimated underwater light or image-forming rays would be complete without mention of certain commonly encountered refractive effects which limit the resolution of fine detail and tend to destroy high collimation. Natural waters often contain refractive nonhomogeneities of two kinds: (1) small scale point-to-point variations in refractive index due, for example, to temperature differences; and (2) transparent biological organisms (plankton) which may range in size from microns to centimeters. The effects of these optical nonhomogeneities has been observed by allowing the beam from the 2-in.-diameter 0.01° divergent lamp shown in Fig. 4 to fall on an underwater viewing screen after traversing any convenient water path or by photographing the effect with an underwater camera having no lens, in the manner

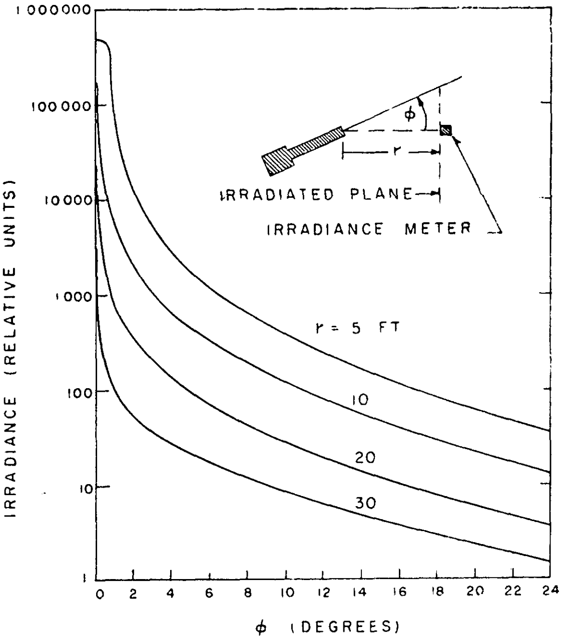

FIG. 20. Irradiance outside a collimated beam of light. Beam divergence: 0.046°; beam diameter: 2-in. Filter: Wratten No. 61. Attenuation length 4.8 ft/ln; Diamond Island.

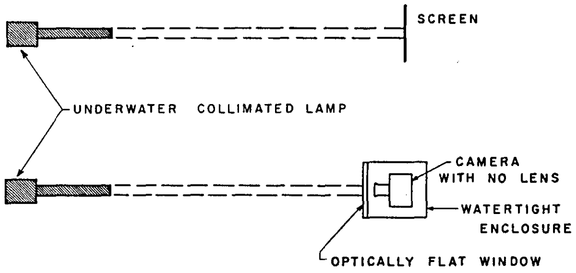

FIG. 21. Techniques for observing (upper figure) and recording (lower figure) the effects of refractive inhomogeneities on the transmission of a highly collimated beam of light through natural water.

suggested by Fig. 21. If such a photograph is made in well-mixed distilled water, only a uniform white field is recorded, but if the distilled water is allowed to stand, a pattern of shadows appears as thermal structures develop. If transparent plankton are added, their refractive shadows are superimposed.

Figure 22 is a photograph of the pattern obtained when such a picture was taken in the clear, natural water at the Diamond Island Field Station in Lake Winnipesaukee, New Hampshire. In this case the light beam passed through 10 ft of lake water. The circular shadows were caused by transparent plankton somewhat less than 1 mm in size whose refractive index differed only slightly from that of water. No effects due to thermal tubulons have been identified in this picture. The light beam was horizontal and 30 in. beneath the surface of the water. A shutter speed of 1/50 second was used because the pattern was in constant restless motion, primarily due to slight wave action, but also due to plankton movements and possibly to thermal drifts.

Loss of resolution. Wavefronts passing through natural waters are distorted by these refractive effects. The edges of objects appear blurred and the apparent contrast of small objects is reduced. Thus, resolving power is impaired and fine details are obliterated. It is said that in some clear, south-sea waters the concentration of transparent plankton is so great that a swimmer cannot distinguish his toes even though his foot is clearly visible at high contrast. Conditions are much less severe at the Diamond Island Field Station, where magnification is necessary to make the loss of resolution obvious.

An experimental study of this loss of resolution was performed several years ago at the Diamond Island Field Station and a theoretical treatment of the effect was evolved.[19,20] At Diamond Island the loss of resolution was comparable to that caused by the on-axis aberrations of a flat water-to-air window of 1/4-in.-thick commercial plate glass when 10 ft of water separated the object from the camera. The angular magnitude of the blur increases as the square root of the object-to-camera distance, and the apparent contrast of fine details is decreased inversely as the third power of the distance in macroscopically uniform water.[20]

DAYLIGHT IN THE SEA

Most of the light in the sea is from the sun and the sky. In sunny weather each square meter of the water surface may be irradiated by as much as one kilowatt of solar power. Approximately 95% of this power en-

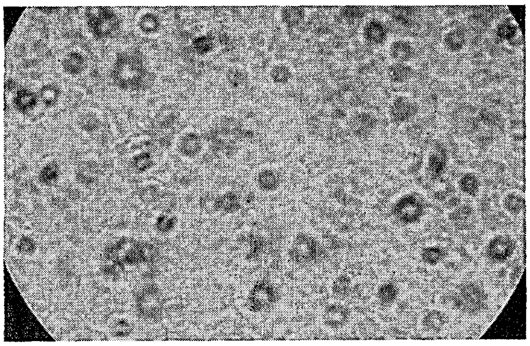

FIG. 22. Photograph of the light distribution from the collimated underwater lamp (Fig. 4) after traversing 10 ft of water in the manner shown schematically in Fig. 21. Camera: Contax without lens. Exposure time: 1/50 sec. Film: Eastman Plus-X. Development: normal, D-76. Beam spread: 0.01°. Beam diameter: 2 in. Attenuation length: 5.6 ft/ln; Diamond Island; 22 August 1961. The diameter of the outer black circular border (caused by the opening in the camera body) measured 1.3 in. on the negative.

[19] S. Q. Duntley, W. H. Culver, F. Richey, and R. W. Preisendorfer, J. Opt. Soc. Am. 42, 877(A) (1952).
[20] S. Q. Duntley, W. H. Culver, F. Richey, and R. W. Preisendorfer, J. Opt. Soc. Am. (to be published).

ters the water and is absorbed somewhere beneath the surface. Daylight is the principal source of energy for the sea, supplying it with heat and supporting its ecology through photosynthesis. Nearly half of the irradiation is infrared, most of which is absorbed within a meter of the surface. As much as one-fifth of the daylight may be ultraviolet and this can penetrate somewhat more deeply if the concentration of dissolved organic decomposition products ("yellow substance") is low. Fortunately, the peak of the solar spectrum is not far from the wavelength (480 mμ) of greatest transparency in clear ocean water. Blue-green light, representing less than one-tenth of the total incident solar power, penetrates so deeply into the sea that it has been detected photoelectrically below 600 m. Visibility, important to inhabitants of the underwater world, is possible chiefly because of this blue-green light.

Directional Distribution of Daylight Underwater

Sunlight entering at the surface becomes progressively more diffuse with depth until a state of diffusion is reached which (1) is characteristic of the water mass, (2) is independent of the solar altitude and the prevailing sky condition, and (3) is invariant with further increases in depth unless optically different water is encountered. This behavior of daylight in water, a subject of conjecture for more than 30 years, was probably first definitively postulated by Whitney[21,22] in brilliant speculations based neither upon adequate radiance distribution data nor upon a valid theoretical analysis but chiefly upon insightful interpretations of irradiance measurements. Whitney's hypothesis could not be confirmed until 1957, when an eight-year experimental program, initiated by the author and conducted in its later stages chiefly by several of his colleagues, culminated in the definitive radiance distribution data of Tyler.[23] These data were obtained with superlative equipment representing nearly a decade of apparatus development. The experiments were conducted in a mountain lake containing optically uniform water of very great depth. This lake (Pend Oreille, Idaho) was used only after many futile attempts had been made to find sufficiently uniform, deep water at sea and in other lakes. Even at Pend Oreille optical uniformity occurs only for a few days during the spring of each year. The Pend Oreille data show an unmistakable, systematic trend toward the formation of a characteristic (or *asymptotic*) distribution of underwater daylight radiance. A series of figures developed from Tyler's tabulated Pend Oreille data[23] and described in the section which follows summarize this experimental evidence for the *asymptotic radiance distribution* hypothesis and illustrate the progressive transformation of the light field from the sunny condition near the surface to the characteristic diffuse distribution which prevails at great depth. A theoretical proof of the existence of characteristic diffuse light (asymptotic radiance distribution) in natural waters has been given by Preisendorfer[24] and confirmatory experimental data in other natural waters have been obtained by Jerlov and Fukuda[25] and Sasaki.[26]

Depth Profiles of Underwater Radiance

The most usable graphical representation of the distribution of daylight radiance in the sea is a family of radiance distribution profiles like those in Fig. 23. Con-

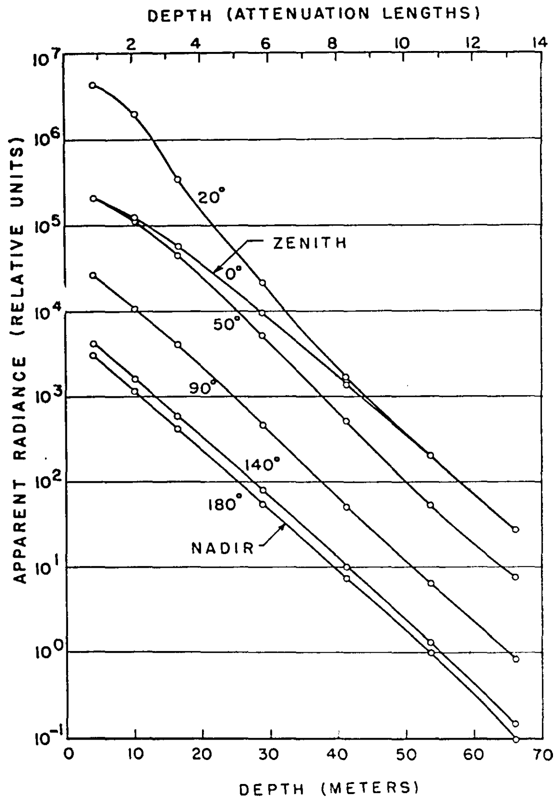

FIG. 23. Depth profiles of underwater apparent radiance for several paths of sight (i.e., zenith angles) in the plane of the sun on a clear, calm, cloudless, sunny day (28 April 1957) at Pend Oreille, Idaho. The circles denote data by Tyler (see reference 23). The solar zenith angle was 33.4°. The submerged photoelectric radiance photometer measured blue light by means of an RCA 931A multiplier phototube equipped with a Wratten No. 45 filter; its field of view was circular and 6.6° in angular diameter. The water was nearly uniform in its optical properties; i.e., the attenuation length (as measured by means of a light beam transmissometer having a tungsten source, an RCA 931A phototube, and a Wratten No. 45 filter) was 2.52 m/ln just beneath the surface and increased very slightly at a steady rate to 2.62 m/ln at a depth of 61 m; that is to say, the change in attenuation length with depth was barely detectable. Additional families of radiance profiles in vertical planes at other azimuths can be constructed from Tyler's tables, which also provide corresponding data for overcast conditions. All such sets of profiles are remarkably similar at great depth. Parallel profiles signify that the radiance distribution has its asymptotic form.

[21] L. V. Whitney, J. Marine Research 4, 122 (1941).
[22] L. V. Whitney, J. Opt. Soc. Am. **31**, 714 (1941).
[23] J. E. Tyler, Bull. Scripps Inst. Oceanog. **7**, 363 (1960).
[24] R. W. Preisendorfer, J. Marine Research **18**, 1 (1959).
[25] N. G. Jerlov and M. Fukuda, Tellus **12**, 348 (1960).
[26] T. Sasaki, Bull. Japan. Soc. Sci. Fisheries **28**, 489 (1962).

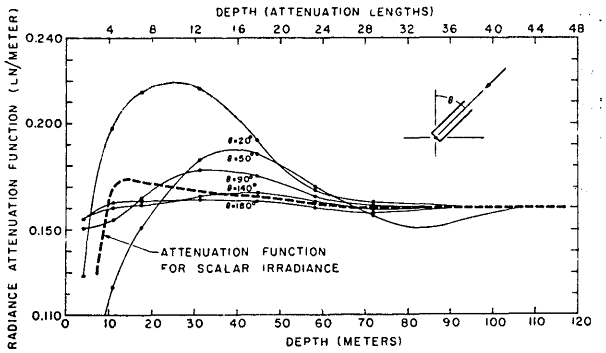

FIG. 24. The solid curves are radiance attenuation functions (i.e., slopes) of the depth profiles of apparent radiance in Fig. 23. The circled points are from Tyler's attenuation function tables (see reference 23). The dashed curve is the attenuation function for scalar irradiance; i.e., the slope of the depth profile of scalar irradiance, a radiometric quantity proportional to the response of a spherical diffuse collector such as that at the top of the instrument pictured in Fig. 25. The transformation of the light field to its asymptotic form is illustrated by the convergence of the radiance attenuation functions to a common, steady value at sufficient depth.

ceptually, each curve represents the results of lowering vertically into the sea a radiance photometer having a fixed zenith angle and azimuth. The unique utility of such profiles arises from the fact that the contrast transmittance of any path of sight in the day-lighted sea is given by the ratio of the apparent background radiances at the *terminals of the path* multiplied by the beam transmittance of the path [see Eq. (8)]. This important general theorem is rigorously true despite any degree of stratification or nonhomogeneity possessed by the water and despite any amount of nonuniformity in the lighting throughout the path of sight. Radiance distribution profiles like those in Fig. 23 enable the apparent background-radiance ratio to be read for any pair of terminal points regardless of the shape of the profile.

In Fig. 23 each curve is nearly, but not quite, straight and nearly, but not quite, parallel with its fellows. When, at sufficient depth, all of the profiles are parallel, the asymptotic radiance distribution prevails.

Radiance Attenuation Functions

The inverse slope of the semilogarithmic underwater radiance distribution profiles in Fig. 23 is called the *radiance attenuation function*. It is symbolized by $K(z,\theta,\phi)$, where z refers to depth, θ specifies the zenith angle of the radiance photometer, and ϕ denotes its azimuth. Figure 24, developed from similar ones by Preisendorfer,[27,28] is a plot of the radiance attenuation functions (slopes) of the radiance profiles shown in Fig. 23. The curves in Fig. 24 have been extrapolated beyond the greatest depth explored by Tyler's measurements in order to illustrate the asymptotic radiance distribution concept more completely. Differential equations for the radiance attenuation functions have been evolved by Preisendorfer.[27]

[27] R. W. Preisendorfer, Scripps Inst. Oceanog. Ref. **58-59**, (1958).

[28] R. W. Preisendorfer, Scripps Inst. Oceanog. Ref. **58-60**, (1958).

Attenuation Function for Scalar Irradiance

The slope of a vertical profile of scalar irradiance $h(z)$, a radiometric quantity measurable by means of a spherical diffuse collector, is called the *attenuation function for scalar irradiance* at depth z and is denoted by $k(z)$. This function is shown by the dashed curve in Fig. 24. The limiting value $k(\infty)$ of $k(z)$ is a convenient experimental parameter for describing the optical properties of the sea because (1) $k(z)$ approaches its asymptotic value at less depth than do the radiance attenuation functions, and (2) it is easier to measure. Figure 25 shows a water-clarity meter proposed by the author and constructed

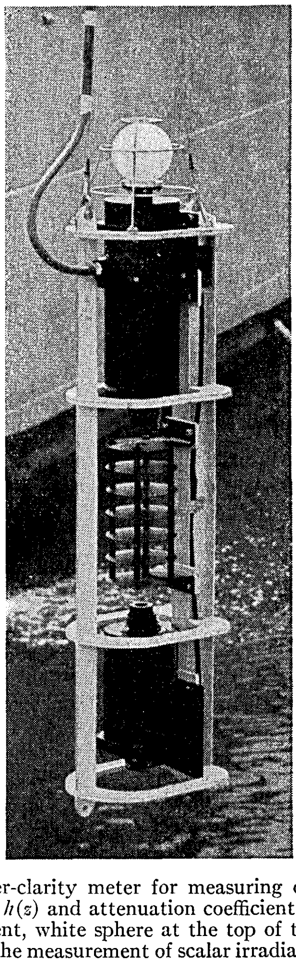

FIG. 25. Water-clarity meter for measuring depth profiles of scalar irradiance $h(z)$ and attenuation coefficient $\alpha(z)$ at sea. The hollow, translucent, white sphere at the top of the instrument is the collector for the measurement of scalar irradiance. Attenuation is measured by means of a highly collimated beam of light, produced by a projector in the lower compartment, which travels upward to a photoelectric telephotometer in the upper chamber. Baffles are used to minimize the effect of daylight in near surface measurements. The use of multiplier phototubes enables this equipment to produce profiles of scalar irradiance at depths greater than 10 attenuation lengths. A pressure transducer is incorporated in the instrument to indicate its depth. Due to the spherical nature of the irradiance sensor, the orientation of the instrument is not important; it can, if desired, be oriented horizontally (see reference 29).

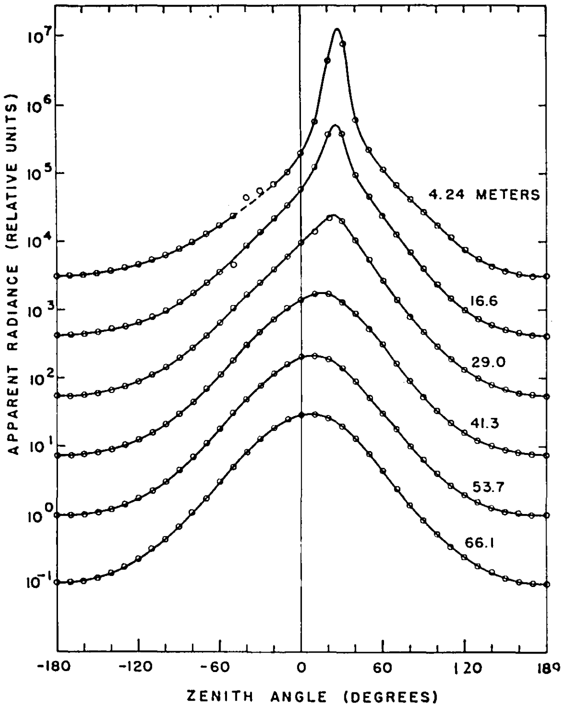

FIG. 26. Underwater radiance distributions in the plane of the sun on a clear, sunny day at depths of 4.24, 16.6, 29.0, 41.3, 53.7, and 66.1 m, respectively. The circles denote data by Tyler (see reference 23) at Pend Oreille, Idaho, 28 April 1957. The solar zenith angle was 33.4° For additional experimental details see Fig. 23. At the shallowest depth measured (4.24 m), the peak of the radiance distribution is at a slightly greater zenith angle than refracted rays from the sun (24.4°); see Fig. 29. At progressively greater depths the distribution becomes less sharply peaked and the maximum moves toward zero zenith angle. The radiance distribution is nearly in its asymptotic form at 66.1 m, the greatest depth at which data were taken. Corresponding trends appear in similar plots of data obtained by Sasaki in ocean water near Japan (see reference 26) and in Gullmar fjord by Jerlov and Fukuda (see reference 25).

by his colleagues,[29] which measures simultaneous vertical profiles of scalar irradiance $h(z)$ and attenuation coefficient $\alpha(z)$ in routine oceanographic surveys.

Shapes of the Underwater Radiance Distribution

The shapes of a typical family of underwater radiance distributions in the plane of the sun at progressively greater depths are shown by Fig. 26, which includes the same data plotted in Fig. 23. At shallow depths the distribution is sharply peaked, approximately in the direction of the refracted rays from the sun. At increasingly greater depths the distribution becomes less sharply peaked and the maximum moves progressively toward the zenith. The change in curve shape is better illustrated by Fig. 27, wherein the upper four curves of Fig. 26 have been superimposed at their respective maxima.

The lower two curves in Fig. 26 do not appear in Fig. 27 because their shape does not differ from that of the 41.3-m curve within the precision of the data. It may be noted, therefore, that the form of the radiance distribution changes throughout only the first 41 m of depth (about 16 attenuation lengths or *optical depths*). At that depth, however, the shift of the maximum toward the zenith is incomplete and continues to change rapidly as depth is progressively increased. Figure 28 shows how the maximum of the underwater daylight distribution shifts toward the zenith with increasing depth; it suggests, by extrapolation, that a depth of 20 attenuation lengths (100 m) or more is required in order for the true asymptotic radiance distribution to be reached.

[29] R. W. Austin, Scripps Inst. Oceanog. Ref. 59-9, (1959).

Irradiance Profiles

When the underwater radiance distribution has its asymptotic form, the irradiance incident on a plane oriented in any direction will decrease exponentially with depth at the same rate as will the irradiance on planes oriented in any other directions. A family of semilogarithmic profiles of the irradiance on planes oriented in various directions is merely a group of parallel straight lines having a slope corresponding to $k(\infty)$, the limiting value of the attenuation function for scalar irradiance. In most ocean water the irradiance $H(z,-)$ on the upper surface of a horizontal plane at any depth z is approximately 50 times as great as the irradiance $H(z,+)$ on the lower surface of the same plane; the irradiance on planes oriented in all other directions at this depth lies between $H(z,-)$ and $H(z,+)$.

At lesser depths, where the underwater radiance distribution departs from its asymptotic form, the semilogarithmic irradiance profiles differ somewhat from parallelism and straightness. Such perturbations are, however, comparatively minor and for many purposes they are negligible. For example, some of the attenuation functions at a depth of 2.5 ft on an overcast day

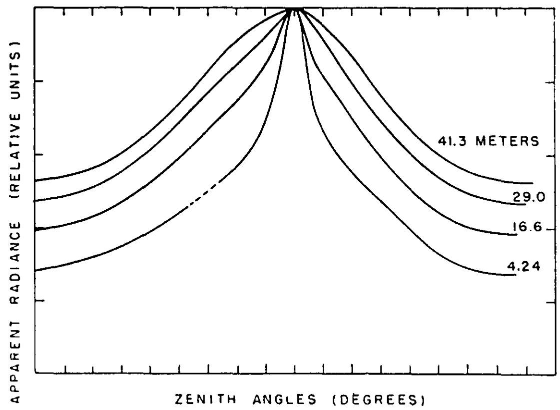

FIG. 27. In this figure the underwater radiance distribution curves for depths 4.24, 16.6, 29.0, and 41.3 m from Fig. 26 have been superimposed at their respective maxima in order to compare their shapes. The radiance curves for depths 53.7 and 66.1 m are not shown since, within the limits of experimental error, their shapes are identical with the curve for 41.3 m depth. Thus, the *shape* of the underwater radiance distribution has nearly completed its transformation to the asymptotic form at 41.3 m depth. The maximum of the curve has not, however, reached zero zenith angle at this depth and is, in fact, changing at maximum rate; see Fig. 28.

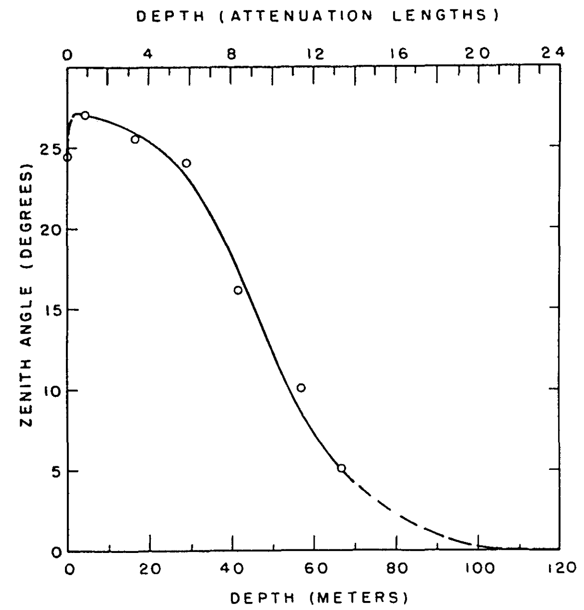

FIG. 28. Illustrating how the peaks of the underwater daylight radiance distributions shown in Fig. 26 shift toward zero zenith angle with increasing depth. At shallow depths in these data the peak occurs at a greater zenith angle than the direction (underwater) of rays from the sun. The extrapolated (dashed) portion of the curve suggests that a depth of more than 100 m is required to bring the peak to zero zenith angle; i.e., to complete the transformation of the light field to its asymptotic form.

(28 August 1959) at Diamond Island were $K(2.5,-)=0.067$ ln/ft, $k(2.5)=0.063$ ln/ft, $K(2.5,+)=0.051$ ln/ft, and $\alpha(2.5)=0.18$ ln/ft.

Contrast Transmittance

Introduction. Underwater sighting ranges are always short compared with sighting ranges in clear air. Nearly all objects, therefore, subtend so large a visual angle when seen underwater that the exact size of the object is of almost no consequence. Except for very tiny objects or the fine details of larger ones, underwater sighting ranges depend almost entirely upon the contrast transmittance of the path of sight when ample daylight prevails. Along horizontal paths of sight dark objects (such as black-suited swimmers) approach detection threshold near the distance $4/\alpha(z)$ when viewed against a water background, although bright objects (including light sources) can be seen further.[30] For objects of sufficient angular size, horizontal daylight sighting ranges underwater are remarkably similar to horizontal daylight sighting ranges in the atmosphere if both are expressed in attenuation lengths. This quantitative similarity does not hold, however, when the path of sight is inclined either upward or downward because water, unlike air, absorbs light so strongly that all aspects of daylight in the sea diminish rapidly with depth. Contrast reduction along inclined paths of sight through optically uniform water are treated after certain general principles have been discussed.

General case. A completely general phenomenological treatment of the reduction of apparent contrast by any scattering and absorbing medium has been given by the author and two of his colleagues in an earlier paper[31] concerned with the atmosphere; Eq. (1) through (10) of that paper and the discussions which accompany them apply also to the reduction of contrast along all underwater paths of sight, and the notation employed in reference 31 has been used throughout the present paper, except that z is used to denote depth (rather than altitude) and is positive from the sea surface downward. Although, in the interest of brevity, only one [Eq. (7)] of those equations is discussed here, they constitute the foundation for all of the relations which follow in this paper.

Equation (7) in reference 31 states that the ratio of the apparent contrast $C_r(z,\theta,\phi)$ of an object at distance r from an observer at depth z along a path of sight having zenith angle θ and azimuth ϕ to the inherent contrast $C_0(z_t,\theta,\phi)$ of a target at depth z_t is

$$C_r(z,\theta,\phi)/C_0(z_t,\theta,\phi)= T_r(z,\theta,\phi)\,{}_bN_0(z_t,\theta,\phi)/{}_bN_r(z,\theta,\phi), \qquad (8)$$

where $T_r(z,\theta,\phi)$ is the beam transmittance of the path of sight for image-forming light and ${}_bN_0(z_t,\theta,\phi)/{}_bN_r(z,\theta,\phi)$ is the ratio of the apparent radiances of the background at the *terminals* of the path of sight. This equation is rigorously true despite any amount of nonuniformity in the water or in its lighting. Profiles of underwater radiance, such as those in Fig. 23, provide the two background radiance values required by Eq. (8) and the beam transmittance can be found from a profile of attenuation length by means of Eq. (16) in reference 31. It should be noted that the beam transmittance $T_r(z,\theta,\phi)$ must include the factor $[n(z)/n(z_t)]^2$ required by geometrical optics when the refractive index $n(z)$ of the medium at the observer differs from that at the target $n(z_t)$, as in the case of underwater observation through a flat face plate or a plane window.

Uniform water. If the underwater path of sight lies entirely within a single optically uniform stratum and if the profile of monochromatic apparent radiance (see Fig. 23) can be approximated by a straight line and represented by the differential equation

$$dN(z,\theta,\phi)/dr=-K(z,\theta,\phi)\cos\theta N(z,\theta,\phi), \qquad (9)$$

where $r\cos\theta=z_t-z$, Eq. (10) of reference 31 can be replaced by differential equations of transfer for spectral field radiance

$$dN(z,\theta,\phi)/dr=N_*(z,\theta,\phi)-\alpha(z)N(z,\theta,\phi), \qquad (10)$$

[30] Along any underwater path of sight a remarkable proportion of the objects ordinarily encountered can be seen at limiting ranges between 4 and 5 times the distance $1/[\alpha(z)-K(z,\theta,\phi)\cos\theta]$, regardless of their size or the background against which they appear, provided ample daylight prevails [see Eqs. (14) and (15)].

[31] S. Q. Duntley, A. R. Boileau, and R. W. Preisendorfer, J. Opt. Soc. Am. 47, 499 (1957).

and for apparent spectral target radiance

$$d_t N(z,\theta,\phi)/dr = N_*(z,\theta,\phi) - \alpha(z)\,{}_tN(z,\theta,\phi). \quad (11)$$

Equations (9), (10), and (11) can be combined and integrated throughout the path of sight to produce the important relation

$$\begin{aligned} {}_tN_r(z,\theta,\phi) = {}&{}_tN_0(z_t,\theta,\phi)\exp[-\alpha(z)r] \\ &+N(z_t,\theta,\phi)\exp[+K(z,\theta,\phi)r\cos\theta] \\ &\times\{1-\exp[-\alpha(z)r+K(z,\theta,\phi)r\cos\theta]\}, \end{aligned} \quad (12)$$

where ${}_tN_r(z,\theta,\phi)$ is the apparent spectral radiance of the target and ${}_tN_0(z_t,\theta,\phi)$ is its inherent spectral radiance. In Eq. (12) the first term on the right represents

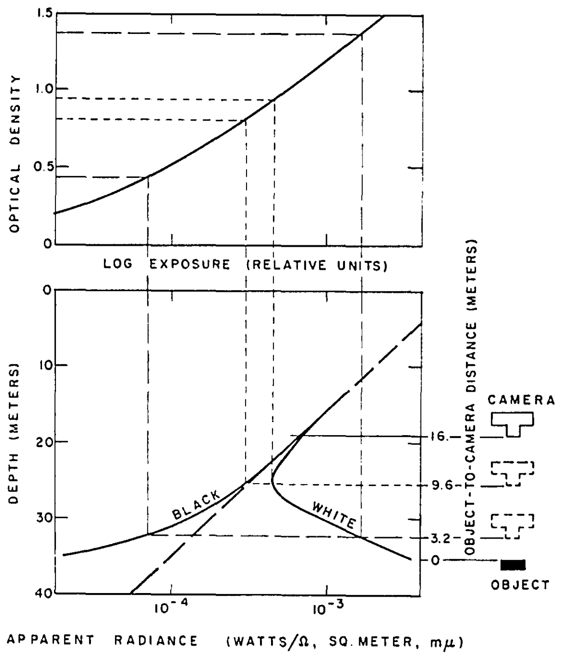

Fig. 29. Illustrating the effect of (vertical) object-to-camera distance on the apparent radiance (lower figure) and the photographic contrast (upper figure) of an object having both white and black areas submerged 35 m beneath the surface of deep, optically uniform water characterized by an attenuation length ($1/\alpha$) of 3.2 m/ln, $(\alpha/K)=2.7$, $H(z,+)/H(z,-)=0.02$, and asymptotic radiance distribution. The prevailing spectral irradiance on the surface of the water is assumed to be 1 W/m², mμ.
As a downward-looking camera is lowered from the sea surface, the apparent radiance presented by the water decreases at the rate of $K=0.116$ ln/m, as shown by the diagonal dashed line in the lower figure. At 19 m depth (i.e., an object-to-camera distance of 16 m or 5 attenuation lengths) the apparent radiances of the object differ but little from that of the surround. When the camera is 9.6 m (i.e., 3 attenuation lengths) above the target, the white area presents an apparent radiance significantly greater than the surround (diagonal dashed line) but the black area appears only slightly darker than the water background. Near this camera position the two terms in the right-hand member of Eq. (12) are equal, so that $dN(z,\pi,0)/dr=0$; at greater camera depths the second term predominates. When the camera is 3.2 m or 1 attenuation length above the object, both the black and the white areas of the target differ markedly in apparent radiance from the surround (diagonal dashed line). The upper figure illustrates, by means of the characteristic curve of a negative material, the range of photographic densities corresponding with object-to-camera distances of 3.2 m (dashed lines) and 9.6 m (dotted lines).

residual image-forming light from the target and the second term represents radiance due to scattering of light in the sea throughout the path of sight, i.e., the *path radiance* $N_r^*(z,\theta,\phi)$. A graphical illustration of Eq. (12) is provided by Fig. 29, which shows how black objects and white objects submerged in deep water appear to emerge gradually from the background as they are approached from above by a descending, downward-looking underwater observer or camera.

In Eq. (12), $\alpha(z)$ and $K(z,\theta,\phi)$ are considered to be constants throughout the path of sight. In uniform water this is true of $\alpha(z)$ but not of $K(z,\theta,\phi)$ unless the radiance distribution is asymptotic. Figure 24 illustrates how $K(z,\theta,\phi)$ changes with z and θ in the plane of the sun; corresponding figures can be constructed from Tyler's tables[23] to illustrate changes with ϕ. Such data should be used to ascertain the variation of $K(z,\theta,\phi)$ on the particular segment of the path of sight to be used; the degree of approximation represented by Eq. (12) [and by Eqs. (14), (15), and (16)] can then be estimated. Because underwater sighting ranges rarely exceed $2/K$, the effect of K variation is seldom appreciable, except near the surface of the sea. General equations, remarkably similar in form to Eqs. (12), (14), (15), and (16), have been written by Preisendorfer (private communication); these involve, for example,

$$\exp\left\{-\int_0^r[\alpha(z)-\cos\theta K(z,\theta,\phi)]dr'\right\}$$

instead of

$$\exp[-\alpha(z)r+\cos\theta K(z,\theta,\phi)r];$$

they are also applicable to nonuniform water and even to multi-media paths of sight.

Equation (12) also specifies the apparent radiance of any background against which a target may be seen; when used for this purpose the presubscript t (for target) should be changed to b (for background). Subtraction of the background form of Eq. (12) from Eq. (12) itself yields the relation

$$\begin{aligned} &{}_tN_r(z,\theta,\phi)-{}_bN_r(z,\theta,\phi) \\ &\quad=[{}_tN_0(z_t,\theta,\phi)-{}_bN_0(z_t,\theta,\phi)]\exp[-\alpha(z)r]. \end{aligned} \quad (13)$$

Equation (13) implies that along *any* underwater path of sight, radiance differences are transmitted with exponential attenuation at the same space rate as image-forming rays.

The two forms of Eq. (12) can be combined with the defining relations for inherent spectral contrast, $C_0(z_t,\theta,\phi)$, and apparent spectral contrast $C_r(z,\theta,\phi)$, which are, respectively,

$$C_0(z_t,\theta,\phi)=[{}_tN_0(z_t,\theta,\phi)-{}_bN_0(z_t,\theta,\phi)]/{}_bN_0(z_t,\theta,\phi),$$

and

$$C_r(z,\theta,\phi)=[{}_tN_r(z,\theta,\phi)-{}_bN_r(z,\theta,\phi)]/{}_bN_r(z,\theta,\phi).$$

When this is done, the ratio of inherent spectral contrast to the apparent spectral contrast is found to be

$$C_0(z_t,\theta,\phi)/C_r(z,\theta,\phi) \\ =1-[N(z_t,\theta,\phi)/{}_bN_0(z_t,\theta,\phi)] \\ \times\{1-\exp[\alpha(z)r-K(z,\theta,\phi)r\cos\theta]\}. \qquad (14)$$

If ${}_bN_0(z_t,\theta,\phi)=N(z_t,\theta,\phi)$, as in the special case of an object suspended in deep water, Eq. (14) reduces to

$$C_r(z,\theta,\phi)=C_0(z_t,\theta,\phi) \\ \times\exp[-\alpha(z)r+K(z,\theta,\phi)r\cos\theta]. \qquad (15)$$

Whenever the underwater daylight radiance distribution has, effectively, its asymptotic form, the radiance attenuation function $K(z,\theta,\phi)$ is a constant, independent of z, θ, and ϕ. Equation (15) may then be written

$$C_r(z,\theta,\phi)/C_0(z_t,\theta,\phi)=\exp[-\alpha+K\cos\theta)]r. \qquad (16)$$

The right-hand member of Eq. (16), sometimes called the *contrast reduction factor*, is independent of ϕ, the azimuth of the path of sight. This and other implications of Eq. (16) were discovered by the author in the course of early experiments as illustrated, in part, by Figs. 30 and 31.

Horizontal paths of sight. Along horizontal paths of sight $\cos\theta=0$ in Eqs. (9), (12), (14), (15), and (16), which show that both the apparent radiance and the apparent contrast of objects seen horizontally underwater change with distance in a manner dependent on α but not on K. When $\cos\theta=0$, Eq. (10) indicates that some unique *equilibrium radiance* $N_q(z,\pi/2,\phi)$ must exist at each point such that the loss of radiance within the horizontal path segment is balanced by the gain, i.e.,

$$dN_q(z,\tfrac{1}{2}\pi,\phi)/dr=0=N_*(z,\tfrac{1}{2}\pi,\phi)-\alpha(z)N_q(z,\tfrac{1}{2}\pi,\phi). \qquad (17)$$

Even in nonuniform water there is an equilibrium radiance for each element of horizontal path although this may differ from point to point. Inclined paths of sight do not have a true equilibrium radiance, as will be clear from Eq. (9), but they possess an exponential counterpart which is illustrated by the diagonal dashed line in Fig. 29.

A method[32] for measuring the attenuation coefficient

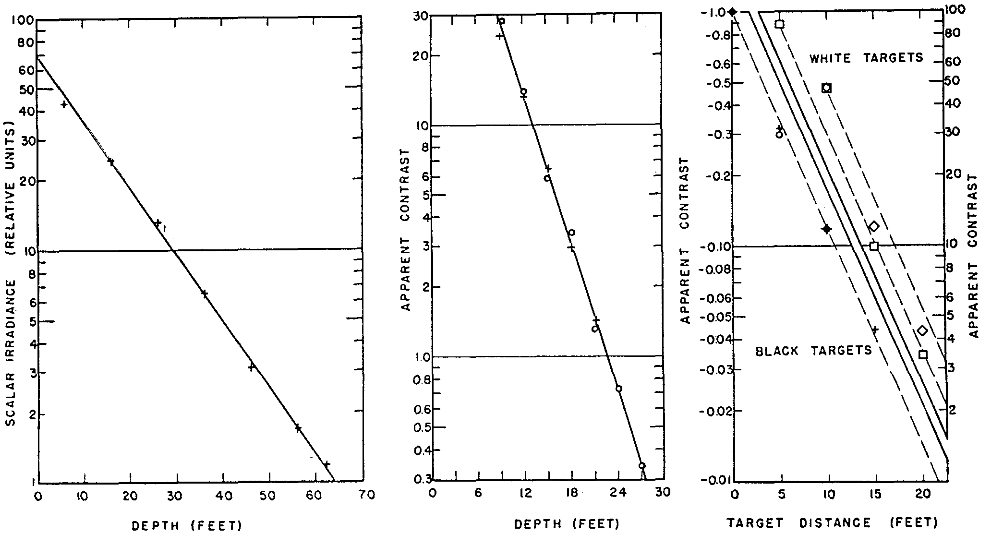

FIG. 30. Interrelated experiments from the September 1948 series at the Diamond Island Field Station: (*Left*) Semilogarithmic depth profile of scalar irradiance obtained by lowering a 6-in.-diameter, air-filled, hollow, translucent, opal glass sphere having a photovoltaic cell sealed in an opening at its bottom. The straightness of the curve indicates optical homogeneity of the water and a depth invariant attenuation coefficient $k(z)=0.066$ ln/ft. (*Center*) Semilogarithmic plot of the absolute apparent contrast of a horizontal, flat, white target lowered vertically beneath a telephotometer mounted in a small, hooded, glass-bottomed boat; calm water, clear sky, low sun. The long, straight portion of the curve illustrates Eq. (15) and its slope indicates that $\alpha(z)+K(z,\pi,0)=0.247$ ln/ft. Because the sun was low the radiance distribution was approximately asymptotic, so that $K(z,\pi,0)\approx k(z)=0.066$ ln/ft and, by subtraction $\alpha(z)=0.181$ ln/ft or the attenuation length $1/\alpha=5.5$ ft/ln. (*Right*) Two semilogarithmic plots of apparent contrast vs target distance along 60°-downward-sloping paths of sight for black targets (lower portion) and white targets (upper portion) have been combined to demonstrate (1) that the apparent contrast is exponentially attenuated with target distance at the same space rate for both light targets and dark targets, (2) that this space rate is independent of azimuth, and (3) that Eq. (16) is valid. All four paths of sight have the same zenith angle, $\theta=150°$, but the azimuth angles relative to the plane of the sun are $\phi=0$ (circled points) and $\phi=45°$ (crosses), $\phi=95°$ (diamonds) and $\phi=135°$ (squares). The dashed straight lines are constructed parallel and, in accordance with Eq. (16), they have a slope $0.181+0.066\cos150°=0.214$ ln/ft. These lines were passed through the uppermost datum point of each series without regard to the lower points; the lines are provided solely to facilitate judgment of the slope and linearity of the data. Photographic underwater telephotometry; green light, calm water, clear sky, low sun.

[32] S. Q. Duntley, J. Opt. Soc. Am. 37, 994(A) (1947) and U. S. Patent No. 2,661,650.

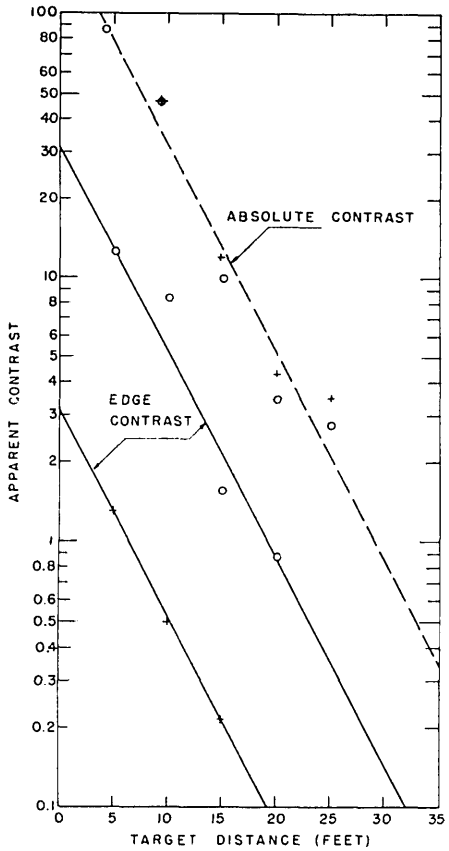

FIG. 31. Comparison of apparent absolute contrast with apparent edge contrast of white targets for two horizontal underwater paths of sight having azimuths relative to the direction of the sun of 95° (crosses) and 135° (circles), respectively. The three lines are parallel and correspond to an attenuation length $1/\alpha = 5.65$ ft/ln. The data are of 24 September 1948 at Diamond Island. Photographic telephotometry; green filter.

$\alpha(z)$ is suggested by Eq. (17) and the fact that in optically uniform water ${}_qN(z,\frac{1}{2}\pi,\phi) = N(z,\frac{1}{2}\pi,\phi)$; thus

$$\alpha(z) = N_*(z,\tfrac{1}{2}\pi,\phi)/N(z,\tfrac{1}{2}\pi,\phi). \quad (18)$$

In Eq. (18), $N_*(z,\frac{1}{2}\pi,\phi)$ can be approximated by the apparent radiance of a very black object, such as an opening in a small black box, located at a unit distance which is small compared with the attenuation length, and $N(z,\frac{1}{2}\pi,\phi)$ is the apparent radiance of the unrestricted water background. This technique is especially convenient for documenting conditions in underwater photography by daylight. The value of $\alpha(z)$ so obtained agrees precisely with data obtained by (1) properly designed light beam transmissometers, (2) measurements of the apparent contrast of underwater objects observed along horizontal paths of sight, and (3) underwater telephotometry of the apparent radiance of the surface of a distant submerged frosted incandescent lamp or other diffusely emitting source.

Field experiments. Experimental explorations of the distribution of daylight in the sea and underwater image transmission phenomena were begun by the author in 1948 and are still in progress. Most of the physical principles discussed in this paper were discovered or generalized early in the course of these experiments. The data guided a collaborative development of the foregoing equations by Dr. Rudolph W. Preisendorfer and the author.[33–35]

Experiments were conducted concurrently in lakes and at sea almost from the beginning because optical principles can be explored better and more inexpensively in lakes whereas the magnitude of the optical constants of ocean waters can be measured only at sea. Most of the data used in this paper to illustrate principles were obtained at a field station established by the author in 1948 at Diamond Island in Lake Winnipesaukee, New Hampshire. Examples of data from the field station are provided in Fig. 30. These data, taken from the 1948 series, illustrate several important principles which are implied and summarized by Eq. (16). Figure 30 shows that the attenuation coefficients $k(z)$ and $\alpha(z)$ obtained by means of a depth profile of scalar irradiance and measurements of the apparent radiance of a white object lowered vertically (in the manner of a Secchi disk) can be used with Eq. (16) to predict the apparent contrast of any object, black or white, along various underwater paths of sight. Measurements of apparent contrast with highly refined photoelectric equipment have been made along many paths of sight and under many kinds of lighting conditions in the course of the field station experiments; all of these experiments support the validity of Eqs. (15) and (16).

The water-clarity meter pictured in Fig. 25 produces a profile of scalar irradiance similar to that shown in Fig. 30 and, therefore, a measure of $k(z)$; it also measures the attenuation coefficient $\alpha(z)$, providing, thereby, the necessary input information for using Eq. (16) to calculate contrast reduction, since $K = k(z)$.

Telephotometry of either black or white targets along any two paths of sight having different inclinations (i.e., zenith angle θ) yields two values of the contrast attenuation coefficient ($\alpha - K\cos\theta$) from which α and K can be found. The use of a horizontal path for determining α, and a downward vertical path for determining $\alpha + K$, is often a convenient choice.

Absolute contrast. The water immediately surrounding a submerged white object sometimes appears to glow. This effect is caused by the intense small-angle forward scattering of light which is reflected by the target in directions adjacent to that of the observer. The effect is most noticeable when a strongly lighted white object is observed against a dark background. The apparent radiance of the scattered glow has been found to be attenuated at the same space rate as the target itself; this is shown by Fig. 31 wherein the semi-logarithmic attenuation curves for apparent *absolute contrast* and apparent *edge contrast* are parallel. Apparent absolute contrast is relative to the apparent background

[33] S. Q. Duntley, Proc. Armed Forces–Natl. Research Council Vision Committee **23**, 123 (1949); **27**, 57 (1950); **28**, 60 (1951).

[34] S. Q. Duntley and R. W. Preisendorfer, MIT Rept. N5ori 07864 (1952).

[35] R. W. Preisendorfer, Scripps Inst. Oceanog. Ref. **58-42** (1957).

radiance that would be observed if the target were absent; apparent edge contrast is relative to the apparent background radiance which appears immediately adjacent to the target. Ordinarily, few underwater objects are white enough to cause the two types of contrast to differ significantly. When the glow is prominent, absolute contrast is usually the more meaningful measure of object detectability, but a full treatment of this topic can be made only in context with details concerning the characteristics of the detector (eye, camera, etc.), a matter beyond the scope of this paper.

Absorption

If radiant power in the sea is to be useful for heating or for photosynthesis it must be absorbed. The monochromatic radiant power absorbed per unit of volume at any depth depends upon the amount of power received by the volume element and the magnitude of the absorption coefficient; i.e., upon the product of the scalar irradiance and the volume absorption coefficient.[36] A more frequently useful relation[37] has been evolved as follows: The net inward flow of radiant power to any element of volume dv in any horizontal lamina of thickness dz at depth z in the sea is

$$\frac{dP(z)}{dv}=\frac{d}{dz}\{H(z,-)-H(z,+)\}$$
$$=\frac{d}{dz}\left\{H(z,-)\left[1-\frac{H(z,+)}{H(z,-)}\right]\right\}. \qquad (19)$$

The ratio $H(z,+)/H(z,-)$, sometimes called the *reflection function* of water, has been found by experiment to be virtually independent of depth and to have a value of 0.02 ± 0.01 for most natural waters unless large quantities of suspended matter are present; the reflection function is rigorously independent of depth when the underwater daylight radiance distribution has its asymptotic form in optically uniform water. To the extent to which 2% effects are negligible, Eq. (19) becomes

$$dP(z)/dv\approx H(z,-)K(z,-), \qquad (20)$$

since, by definition, $K(z,-)=-[dH(z,-)/dz]/H(z,-)$. Thus, the radiant power absorbed per unit of volume at any depth in the sea can be measured simply by lowering an upward-facing, diffusely collecting, flat photocell and determining the product of the magnitude and slope of the resulting profile of downwelling irradiance, as illustrated by Fig. 32.

Alternatively, the quantity $\{H(z,-)-H(z,+)\}$ can be measured directly by lowering an assembly of two diffusely collecting, flat photocells mounted back to back so that one faces upward and the other downward. Such an assembly, sometimes called a *janus cell*, can be used to measure $dP(z)/dv$ by means of Eq. (19) in turbid waters for which $\{1-[H(z,+)/H(z,-)]\}$ is not negligible.

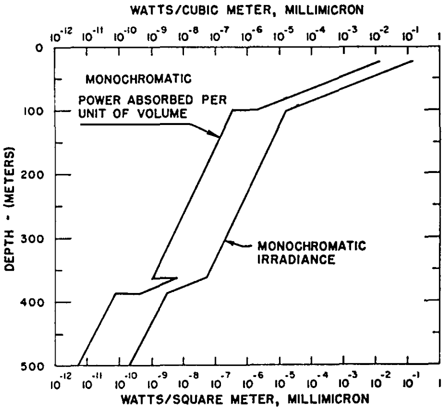

FIG. 32. Superimposed semilogarithmic plots of monochromatic downwelling irradiance vs depth and monochromatic radiant power absorbed per unit of volume vs depth illustrate the (approximate) relation between these quantities expressed by Eq. (20). Monochromatic downwelling irradiance is the total monochromatic radiant power per unit of area received by the upper surface of a horizontal plane at arbitrary depth z. The product of this irradiance and its depth attentuation function (slope of its depth profile) is, within about 2%, equal to the monochromatic power absorbed per unit of volume. Thus, at a depth of 50 m in Fig. 32, $H(50,-)=6.3\times10^{-3}$ W/(m^2, mμ), $K(50,-)=0.114$ ln/m, and $dP(50)/dv\approx(6.3\times10^{-3})(0.114)=7.2\times10^{-4}$ W/(m^3, mμ). Neither of the curves in this figure represent specific experimental data, but the irradiance profile is typical of the Pacific Ocean off California. The presence of a deep scattering layer is shown below 350 m.

CONCLUSION

Although no research program is ever fully completed and the author hopes to participate in studies of light in the sea for many years to come, the investigations which, with many colleagues, have been made thus far, coupled with the findings of other workers all over the world, have produced a sufficient quantitative understanding of the optical properties of ocean water and the behavior of underwater light to provide scientific guidance and optical engineering methods for those persons whose interests or occupations involve light in the sea.

ACKNOWLEDGMENTS

The long research program, spanning two decades, from which this paper is drawn has involved too many persons to permit complete acknowledgment here. Special mention should be made, however, of the important technical contributions of Dr. David L. MacAdam, Willard P. Greenwood, Capt. Dayton R. E. Brown, Professor George E. Russell, John Frankovitch, Frederick C. Spooner, Robert W. Sandberg, Walter Rutkowski, Robert J. Uhl, Frances Richey, Dr. Rudolph W. Preisendorfer, Roswell W. Austin, Almerian R. Boileau, John E. Tyler, Justin J. Rennilson, William Hadley Richardson, Dr. William H. Culver, Theodore J. Petzold, Charles W. Saunders, Jr., Sidney Lindroth, Alden D. J. Hooton, Roger A. Howerton, and Clarence Fred Pinkham who, since 1949, has superintended nearly all of the field operations.

[36] R. W. Preisendorfer, Scripps Inst. Oceanog. Ref. 58-41, (1957).

[37] S. Q. Duntley, Natl. Acad. Sci./Natl. Research Council Publ. 473, 85 (1956).